High-fidelity geometry models for improving the consistency of CHAMP, GRACE, GOCE and Swarm thermospheric density data sets

March, G.; Doornbos, E. N.; Visser, P. N.A.M.

DOI
10.1016/j.asr.2018.07.009

Publication date
2019

Document Version
Final published version

Published in
Advances in Space Research

Available online at www.sciencedirect.com

ScienceDirect

Advances in Space Research 63 (2019) 213–238

ADVANCES IN SPACE RESEARCH (a COSPAR publication)

www.elsevier.com/locate/asr

High-fidelity geometry models for improving the consistency of CHAMP, GRACE, GOCE and Swarm thermospheric density data sets

G. March [*,1], E.N. Doornbos [1], P.N.A.M. Visser [1]

Department of Astrodynamics and Space Missions, Faculty of Aerospace Engineering, Delft University of Technology, Kluyverweg 1, 2629 HS Delft, Netherlands

Received 22 May 2018; received in revised form 10 July 2018; accepted 12 July 2018
Available online 20 July 2018

Abstract

During the last two decades, accelerometers on board of the CHAMP, GRACE, GOCE and Swarm satellites have provided high-resolution thermosphere density data to improve our knowledge on atmospheric dynamics and coupling processes in the thermosphere-ionosphere region. Most users of the data have focused on relative density variations. Scale differences between datasets and models have been largely neglected or removed using ad hoc scale factors. The origin of these scale differences arises from errors in the aerodynamic modelling, specifically in the modelling of the satellite outer surface geometry and of the gas-surface interactions. Therefore, the first step to remove the scale differences is to enhance the geometry modelling. This work forms the foundation for the future improvement of characterization of satellite aerodynamics and gas-surface interactions models at TU Delft, as well as for extending the use of sideways and angular accelerations in the aerodynamic analysis of accelerations and derivation of thermosphere datasets. Although work to improve geometry and aerodynamic force models by other authors has focused on CHAMP and GRACE, this paper includes the GOCE and Swarm satellites as well. In addition, it uses a density determination algorithm that is valid for arbitrary attitude orientations, enabling a validation making use of attitude manoeuvres. The results show an improvement in the consistency of density data between these four missions, and of data obtained before, during and after attitude manoeuvres of CHAMP and Swarm. The new models result in larger densities, compared to the previously used panel method. The largest average rescaling of density, by switching to the new geometry models is reached for Swarm at 32%, the smallest for GRACE at 5%. For CHAMP and GOCE, mean differences of 11% and 9% are obtained respectively. In this paper, an overview of the improvements and comparisons of data sets is provided together with an introduction to the next research phase on the gas-surface interactions.

Keywords: Thermosphere; Atmospheric drag; Density; Accelerometer; Geometry modelling; Aerodynamic modelling; DSMC

1. Introduction

The accuracy of tracking- and accelerometer-derived thermospheric density data sets is closely connected to satellite drag modelling. The previous generation of thermospheric density data sets used simplified satellite geometries (Sutton, 2008; Doornbos, 2011). These geometries are commonly characterized by a limited number of flat panels, which aim to describe the full satellite outer surface geometry. Weaknesses in these models turned out to adversely affect the accuracy and consistency of the derived densities. Large scale differences between data sets and atmospheric models have been detected. Until now, these discrepancies have been neglected or removed using specific scale factors (Bowman et al., 2008; Weimer et al., 2016). However, more

* Corresponding author.
E-mail addresses: g.march@tudelft.nl (G. March), E.N.Doornbos@tudelft.nl (E.N. Doornbos), P.N.A.M.Visser@tudelft.nl (P.N.A.M. Visser).
[1] Faculty of Aerospace Engineering, Delft University of Technology.

https://doi.org/10.1016/j.asr.2018.07.009
0273-1177/

accurate thermospheric densities require improved satellite geometry models and rarefied flow analysis on these models. Once the geometry and aerodynamic models are enhanced, high fidelity drag coefficients can be computed to provide new density estimations.

In general, aerodynamic coefficients or ballistic coefficients can be obtained either by estimating them from tracking data during orbit determination, or by analytically or computationally modelling the aerodynamics for defined satellite geometries. When estimating drag coefficients from orbit tracking data, errors in the thermosphere density model that was used will affect the estimate. In many cases, this is desirable, for example when using the estimate for subsequent orbit predictions, based on e.g., GPS, S-Band or satellite laser ranging tracking. If the drag coefficient is used to generate independent density data sets however, it should be free of such model dependencies. Emmert (2009) applied the relations between Two-Line Element (TLE data) and thermosphere density of Picone et al. (2005), and resolved constant per-object ballistic coefficients for approximately 5000 objects in the process, based on the physical drag coefficient of one spherical reference object. For non-spherical objects, a higher fidelity modelling solution is required. If the satellite shape can be approximated by a combination of elementary shapes, this can be obtained with a closed-form analytical approach (Sentman, 1961a, b). Otherwise, a simulation of aerodynamic effects on detailed satellite geometries with physics-based rarefied gas dynamics solvers (i.e. Bird, 1994) is required. The analytical approach is accurate only for simple geometries (i.e. flat panel, sphere, cylinder, cube), which usually do not fully describe an operational satellite. Whereas, the computational methods can analyse complex shapes and provide more accurate information.

Throughout this work, physical drag coefficients have been determined for different scenarios, in order to improve current density datasets. The technique presented in this paper provides the opportunity to enhance the estimation of force coefficients and, consequently, satellite aerodynamics. The obtained improvement over the selected missions increases the understanding of the thermospheric region and new density data sets are provided as an outcome of this research.

The implemented methodology is summarized in Section 2. The adoption of a high fidelity geometry model is crucial for estimating aerodynamic coefficients. Therefore, for the introduced set of satellites, new geometries have been designed by making use of available technical drawings and pre-launch photographs. A description of the geometry modelling can be found in Section 3. The following aerodynamic investigation uses the output of this first modelling phase.

The satellite aerodynamic forces are computed by a rarefied gas dynamics simulator based on the Direct Simulation Monte Carlo (DSMC) technique (Bird, 1994). Section 4 presents validations and comparisons. In order to simulate rarefied atmospheric flows, it is also possible to use additional approaches. One of those is the Test Particle Monte Carlo (TPMC) method (Davis, 1960). Together with the DSMC, it is one of the most common techniques used for rarefied flow simulators. Both methods can treat multiple reflections and shadowing, but have the main limitation of being computationally expensive. The TPMC model interacts with the surface elements but does not implement intermolecular collisions. This makes simulations faster than common DSMC computations. However, for both methods, atmospheric particles impinge on surfaces with velocities that are computed using a Maxwellian velocity distribution. The energy exchange between molecules and surface elements is computed and resulting forces can be processed.

Within the last years, numerous works have been performed on satellite aerodynamics by Monte Carlo techniques and there is an increasing interest in processing satellite data with high fidelity geometries. In Pilinski et al. (2016), a similar approach to the method presented in this paper is applied to the DANDE satellite. The SPARCS software (Pilinski, 2011), based on the test particle technique, analyses a triangulated mesh to provide aerodynamic coefficients. The numerical test-particle technique has been used also by Mehta et al. (2017) for the CHAMP and GRACE satellites. In this work, data have been processed with new improved geometries. Results show average differences with respect to the panellized models previously in use in Delft (Doornbos, 2011) of 14–18% for CHAMP and 10–24% for GRACE.

In this work, different assumptions have been made and in addition to CHAMP and GRACE, also the GOCE and Swarm satellites have been investigated. The main mission details are listed in Table 1, whereas an overview of the altitudes evolution within the satellite lifetimes is provided in Fig. 1. Section 5 describes all the differences between these approaches and the resulting densities in detail. Multiple comparisons with existing data sets and atmospheric models are available. Section 6 provides conclusions and an outlook on future work.

Table 1
List of the mission characteristics for the CHAMP, GRACE, GOCE and Swarm satellites.

Satellite	CHAMP	GRACE-A, -B	GOCE	Swarm-A, -C	Swarm-B
Operator	DLR	NASA/DLR	ESA	ESA	ESA
Launch date	Jul. 2000	Mar. 2002	Mar. 2009	Nov. 2013	Nov. 2013
End of the mission	Sept. 2010	Oct. 2017	Oct. 2013	–	–
Initial altitude	460 km	505 km	270 km	470 km	530 km
Inclination	87.3 deg	89.0 deg	96.7 deg	87.4 deg	87.8 deg

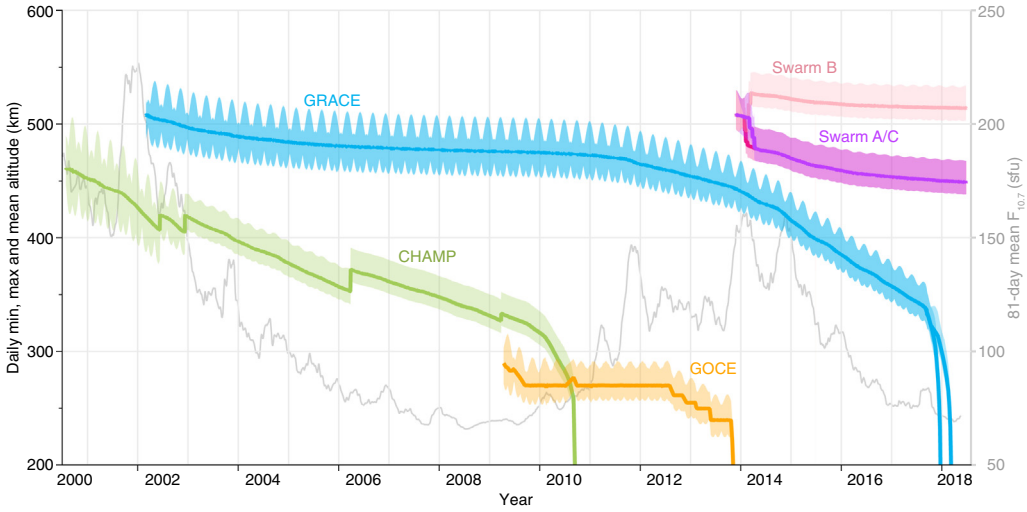

Fig. 1. CHAMP, GRACE, GOCE and Swarm altitudes evolution.

2. Methodology

Satellite aerodynamic forces and torques can be estimated as a function of many inputs. The atmospheric density is a crucial contribution among them. In this paper, the reverse process is used to provide an improved density data set starting from a detailed aerodynamic modelling. Starting from the expression of the aerodynamic drag acceleration (Bruinsma et al., 2004), the following equation allows to calculate the atmospheric density.

$$\rho = \frac{2\, m\, a_{drag}}{C_D\, A_{ref}\, V_{rel}^2} \tag{1}$$

In Eq. (1), ρ is the neutral mass density, m the satellite mass, a_{drag} the drag acceleration, C_D the drag coefficient, A_{ref} a reference area and V_{rel} the velocity relative to the atmosphere. This equation highlights the direct influence of drag coefficients on the density estimation accuracy.

Previous estimations of the neutral mass density have been processed with force coefficients generated from panellized satellite geometries. However, the inability to model multiple reflections and shadowing effects introduced systematic errors at the level of 5–15% (Doornbos, 2011). In general, the panel method consists of the application of Sentman's equations for flat panels to simplified geometries constructed from multiple panels with different orientations (Sentman, 1961a,b). A limited number of flat panels describe the entire structure of the satellite. Normal vectors and areas of each panel provide the fundamental information needed to retrieve aerodynamic coefficients.

Within this paper, the aerodynamic modelling is enhanced using the DSMC approach in combination with high fidelity geometries. Satellite accelerations are reprocessed leading to higher fidelity densities in better agreement with atmospheric models. Panel model geometry and aerodynamic modelling turned out to reduce the reliability of derived densities, especially for satellites with complex shape.

The use of DSMC introduces flexibility for analysing not only free-molecular regimes, but also transition to continuum flow in re-entry conditions for additional research scenarios. In particular, the Stochastic Parallel Rarefied-Gas Time-Accurate Analyzer (SPARTA) simulator from SANDIA Laboratories (Gallis et al., 2014) is used in this work for the aerodynamic modelling. The collisions between atmospheric particles and satellite outer surfaces are simulated within a fixed domain. Pressures and shear stresses associated to each surface element are computed and processed to retrieve overall satellite force coefficients. Aerodynamic data sets from this processing are obtained as a preliminary output. For each analysed configuration, the computed coefficients in the aerodynamic and body fixed frames are listed together with the characteristic simulation inputs (i.e. speed ratio, Euler angles). These data sets are successively processed to obtain atmospheric densities. Further details about the process of extracting densities from accelerometer data can be found in Section 5 and in Doornbos (2011). For the Swarm satellites, GPS-derived accelerations have been used instead of accelerometer data due to the presence of numerous spikes and anomalies (Siemes et al., 2016). These alternative accelerations are estimated within the orbit determination processing using a Kalman-filter approach (Wermuth et al., 2010). In particular, Swarm densities resulting from this procedure were already analysed during the June 2015 geomagnetic storm in Astafyeva et al. (2017).

In this paper, for the complete set of satellites, accelerations have been processed with panel and SPARTA-DSMC methods in order to analyse discrepancies between the two approaches. Further comparisons have been performed with a set of semi-empirical atmospheric models. The achieved results are provided in Section 5.

3. Geometry modelling

The low level of information about existing panel model surfaces is a significant problem for properly modelling satellite aerodynamics. Within this paper, the CHAMP-TU Delft (Doornbos, 2011), GRACE-Bettadpur (Bettadpur, 2007), GOCE-Alenia (Cometto, 2007) and Swarm-Astrium (Siemes, 2018) have been used for the panel model geometries. These macro model surfaces are respectively characterized by 16 panels for CHAMP, 12 for GRACE, 44 for GOCE and 15 for Swarm. Further details about these models and others can be found in Tables 2 and 3. In general, for each panel, information about normal vector components, area, reflectivity, diffusivity and emissivity indexes are listed in the macro models. Information about panels relative locations are not provided. For this reason, multiple reflections and shadowing effects are not easy to implement within this method. Moreover, for this model, complex instruments like protruding antenna or beams turned out to be difficult to model with a satisfactory accuracy.

As input for SPARTA-DSMC, new high fidelity geometry models were designed. These geometries are the inputs for the SPARTA-DSMC simulations, which will be discussed in the next Section 4. In order to reproduce satellite geometries with high fidelity, technical drawings (Schulz, 1999; Luehr, 2000; Hess, 2001; Bettadpur, 2012; Severino, 2004a,b; Hammond, 2006) have been used and compared with the generated surfaces. An overview of the new geometry models is available in Fig. 2. Qualitative and quantitative comparisons with technical drawings and the previous panel models are available in Appendix A and in Table 3. In order to raise the reliability, all the possible outer surface elements have been implemented in the geometry modelling. For this reason, technical drawings from satellite manufacturing companies and pre-launch pictures have been exploited in order to correctly model structures, coatings, thermal blankets and further details, which were not implemented in previous models. Table 3 shows small differences in the projected areas along the spacecraft body-fixed axes for GRACE and GOCE. These discrepancies reach a maximum value of 6% with respect the newly designed geometries. Larger differences are highlighted for CHAMP. This is especially verified comparing the projected areas along X-axis for Luehr (2002) and Bruinsma and Biancale (2003), which register differences of 40.3% and 19.1% respectively. These higher percentages are consistent with similar comparisons in Doornbos (2011). The Swarm satellites show the largest differences with respect to the new model. The highest contribution in the discrepancy is associated to the X-axis projection which has a much smaller area with respect to the Astrium geometry model.

Table 3
Projected areas (in m^2) of the CHAMP, GRACE, GOCE and Swarm satellites as viewed along the spacecraft body-fixed axes for different sources. Percentages provide the comparisons with the new designed geometries. The direction of X is along-track, whereas for Y and Z are along cross-track and nadir orientations respectively.

Satellite	Ref. ID	X	[%]	Y	[%]	Z	[%]
CHAMP	1	0.787		3.193		6.540	
	2	0.742	−5.7	3.120	−2.3	6.444	−1.5
	3	0.794	+0.9	3.245	+1.6	6.621	+1.2
	4	0.470	−40.3	3.377	+5.8	6.295	−3.7
	5	0.637	−19.1	3.377	+5.8	6.295	−3.7
	6	0.743	−5.7	3.122	−2.2	6.456	−1.3
GRACE	7	1.008		2.488		6.103	
	8	1.001	−0.6	2.463	−1.0	-	-
	9	1.043	+3.5	2.550	+2.5	6.153	+0.8
	10	1.001	−0.6	2.638	+6.0	6.365	+4.3
GOCE	11	1.038		10.738		5.759	
	12	1.035	−0.3	11.210	+4.4	6.049	+5.0
Swarm	13	0.784		3.181		6.517	
	14	1.497	+90.9	3.381	+6.3	5.081	−22.0

4. Aerodynamic modelling

The accelerometers on board of the CHAMP, GRACE, GOCE and Swarm satellites provide measurements of

Table 2
List of the satellite models with reference ID and description.

Satellite	ID	Title	Description	Reference
CHAMP	1	SPARTA-March	3D model	This work
	2	CH-IT-DID-001	Tech. drawings, panel model	Luehr (2000)
	3	ANGARA-CH	3D model	Doornbos et al. (2009)
	4	Luehr	Panel model	Luehr (2002)
	5	Bruinsma	Panel model	Bruinsma and Biancale (2003)
	6	TU Delft	Panel model	Doornbos (2011)
GRACE	7	SPARTA-March	3D model	This work
	8	CSR-GR-03-02	Panel model	Bruinsma and Biancale (2003)
	9	ANGARA-GR	3D model	Doornbos et al. (2009)
	10	Bettadpur	Panel model	Bettadpur (2007)
GOCE	11	SPARTA-March	3D model	This work
	12	Alenia	Tech. drawings, Panel model	Cometto (2007)
Swarm	13	SPARTA-March	3D model	This work
	14	Astrium	Panel model	Siemes (2018)

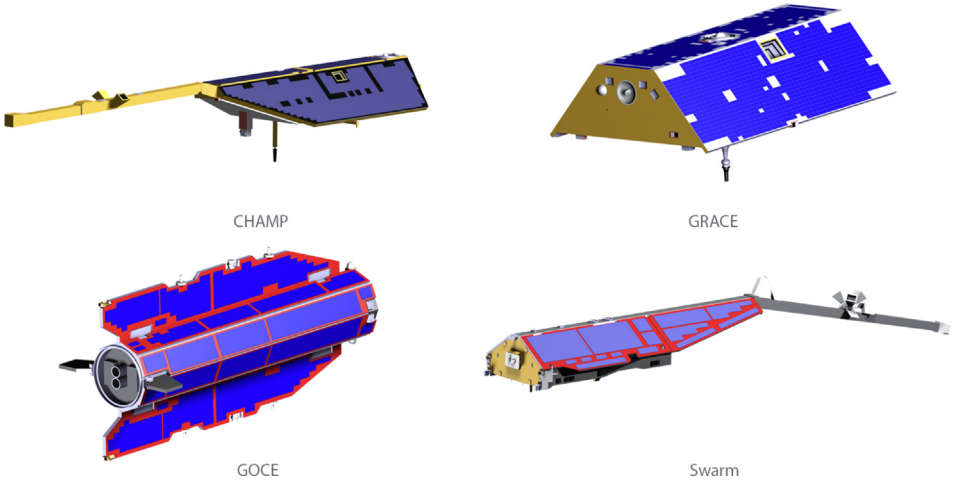

Fig. 2. Rendering of satellite geometry models designed with CATIA V5 R21.

non-gravitational accelerations. The measured accelerations contain several contributions, which are not exclusively related to atmospheric drag. In order to process satellite aerodynamics from accelerometer data, a correct modelling of additional contributions needs to be performed. In addition to the aerodynamic, other accelerations are associated to solar radiation pressure, Earth infra-red radiation pressure, Earth albedo radiation pressure and propulsive thrust. Once all these accelerations are modelled as in Doornbos (2011), the aerodynamic accelerations can be retrieved. In lack of reliable accelerations from the accelerometers, GPS data processing can also provide the necessary information about non-gravitational forces (Van den IJssel, 2014). This method has been already implemented for deriving Swarm L2 density products (Doornbos et al., 2017) and is used as well in this research.

For the analysed missions, the molecules are at large distances from each other, guaranteeing free molecular flow regime. This allows us to neglect particle-particle collisions, which speeds up DSMC simulations. In this work, the aerodynamic coefficients are provided by the SPARTA simulator. The performed simulations cover several different characterizations of thermospheric flows. Moreover, within a specific domain, several attitude configurations have been simulated in order to describe all possible scenarios encountered throughout the mission lifetime. Specific ranges for both attack and side-slip angles have been introduced depending on each spacecraft operational history.

Once that geometry modelling has been improved, the influence of gas-surface interactions between particles and satellite surfaces on the aerodynamic accelerations is crucial to be investigated. One of the most important parameters for this investigation is the energy accommodation coefficient (α_E). This parameter provides information about the energy exchange between atmospheric particles and satellite outer surfaces (Pilinski et al., 2016) and at this point will be an input of the new aerodynamic model. If the particles retain their mean kinetic energy after the collision, this parameter is zero, whereas if particles adjust their temperature to the satellite surface temperature, this coefficient reaches 1. The energy accommodation coefficient is defined as follows:

$$\alpha_E = \frac{T_{inc} - T_{re}}{T_{inc} - T_w} \tag{2}$$

Within this formula, T_{inc} is the particles temperature before the collision, T_{re} the re-emitted particles temperature and T_w the satellite outer surface temperature. The thermosphere is influenced by quasi-diffusive gas-surface interactions. The α_E value depends on different factors like solar activity, altitude and adsorbed gas composition over satellite surfaces (Pilinski et al., 2013; Pardini et al., 2010). In order to fix an accommodation coefficient to focus exclusively on geometry and aerodynamic modelling, an ideal fully-diffusive reflection mode (α_E=1) has been selected for this study. The implementation of a detailed gas-surface interactions model with the introduction of optimal accommodation coefficients is an important next step for the research described in this paper.

The energy accommodation coefficient has been introduced in Sentman's equation, and consequently in the panel method, by Moe et al. (2004) and Sutton (2009) as well as Doornbos (2011) for accelerometer data processing.

The relative velocity (V_r) is defined as the velocity of the satellite with respect to the surrounding atmosphere. Following this implementation, the drag unit vector ($\hat{u}_D$) and the $\vec{V}_r$ vectors have the same direction, whereas the lift unit vector for each single panel ($\hat{u}_{L,i}$) can be found by Eq. (3), where $\hat{n}_i$ is the normal vector of the i-th flat plate element. The negative dot products of drag and lift unit vectors with $\hat{n}_i$ are defined as γ_i and l_i respectively.

$$\hat{u}_{L,i} = -\frac{(\hat{u}_D \times \hat{n}_i) \times \hat{u}_D}{\|(\hat{u}_D \times \hat{n}_i) \times \hat{u}_D\|} \tag{3}$$

In order to retrieve information about drag and lift, Sentman's formulas for a single-sided flat plate can be modified using Eqs. (4) and (5),

$$C_{D,i,j} = \left[\frac{P_{i,j}}{\sqrt{\pi}} + \gamma_i Q_i Z_{i,j} + \frac{\gamma_i}{2}\frac{v_{re}}{v_{inc}}\left(\gamma_i\sqrt{\pi}Z_{i,j} + P_{i,j}\right)\right]\frac{A_i}{A_{ref}} \quad (4)$$

$$C_{L,i,j} = \left[l_i G_j Z_{i,j} + \frac{l_i}{2}\frac{v_{re}}{v_{inc}}\left(\gamma_i\sqrt{\pi}Z_{i,j} + P_{i,j}\right)\right]\frac{A_i}{A_{ref}} \quad (5)$$

where

$$\gamma_i = -\hat{u}_D \cdot \hat{n}_i \qquad l_i = -\hat{u}_L \cdot \hat{n}_i \quad (6)$$

$$G_j = \frac{1}{2s_j^2} \qquad P_{i,j} = \frac{1}{s_j}\exp(-\gamma_i^2 s_j^2)$$

$$Q_j = 1 + G_j \qquad Z_{i,j} = 1 + erf(\gamma_i s_j) \quad (7)$$

The j-index is related to the j-th constituent. The overall aerodynamic coefficients consist in the weighted sum of major constituents of local atmosphere. Furthermore, in the previous equations, the velocity ratio between re-emitted and incoming particles (v_{re}/v_{inc}) is obtained as a function of the energy accommodation coefficient and wall temperature by Eq. (8) from Koppenwallner (2009).

$$\frac{v_{re}}{v_{inc}} = \sqrt{\frac{1}{2}\left[1 + \alpha_E\left(\frac{4RT_w}{v_{inc}^2} - 1\right)\right]} \quad (8)$$

Within atmospheric flow investigations, the speed ratio (s) has a crucial importance. This parameter is the ratio between satellite speed (v_{inc}) and the most probable speed of the atmospheric particles (denominator of Eq. (9)). Analytically, the Eq. (9) provides the mentioned parameter.

$$s = \frac{v_{inc}}{\frac{\sqrt{\gamma RT_{inc}}}{m}} \quad (9)$$

From the previous formula, it is possible to see that the speed ratio is directly connected with the satellite speed, local atmospheric temperature (T_{inc}), molecular mass (m) and gas constant (R). Analysing a certain range of speed ratios, including attitude variations as well, all encountered mission scenarios can be simulated. For the selected satellites, within the performed simulations, the speed ratio ranges between 1 and 14. This interval guaranteed a complete description of experienced thermospheric conditions. After a validation, provided in next Section 4.1, results concerning satellite aerodynamics are presented in Section 4.2.

4.1. Validation

In order to validate SPARTA computations, simple geometries have been introduced and compared with panel method results. In this Section, two validations for a flat panel and a box are presented. Fig. 3 gives a first comparison between the panel method result (solid lines) and SPARTA aerodynamic coefficients (markers) for a two-sided flat panel. At 0 degree of attack angle, the normal vector is aligned with the atmospheric flow direction and the drag force reaches its maximum value. Fig. 4 shows the same analysis for a box with angle of attack (a) and side-slip (b) angle variations. The aerodynamic coefficients have been normalised with a reference area set to 1 m^2.

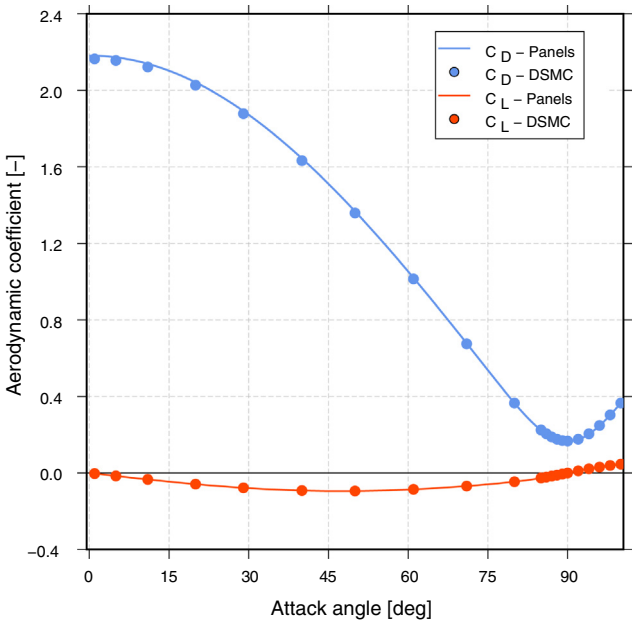

Fig. 3. SPARTA validation for a two-sided flat plate. Aerodynamic coefficients computed using the panel method (solid lines) are compared with DSMC computations (markers).

For both investigations, the two approaches turned out to be in good agreement. The presented simulations in Figs. 3 and 4 have been performed for a fixed speed ratio equal to 7, atmospheric temperature of 1000 K and satellite surface temperature of 400 K. The atmospheric composition is assumed to be 100% atomic oxygen. Changes in selected inputs do not modify the agreement between the two approaches. In combination with the presented validations, a sensitivity analysis has been performed. This study showed a relevant influence of energy accommodation coefficient and molecular mass on aerodynamic coefficients in agreement with Doornbos (2011). Whereas, for temperatures the influence is smaller, especially for the surface temperature, which is not significantly affecting computed coefficients.

4.2. Satellite aerodynamics

In order to compare the panel and SPARTA methods for realistic satellite aerodynamics, normalised force coefficients as a function of attack and side-slip angle have been investigated. A representation of the analysed angles is available in Fig. 5. In the following results, inputs are assumed to be the same as the previously defined validations (Section 4.1). However, additional settings are also tested at the end of this section. Figs. 6 and 7 show the drag, lift and lift over drag ratio for CHAMP. Fig. 6 analyses attack angle influence, whereas Fig. 7 shows the

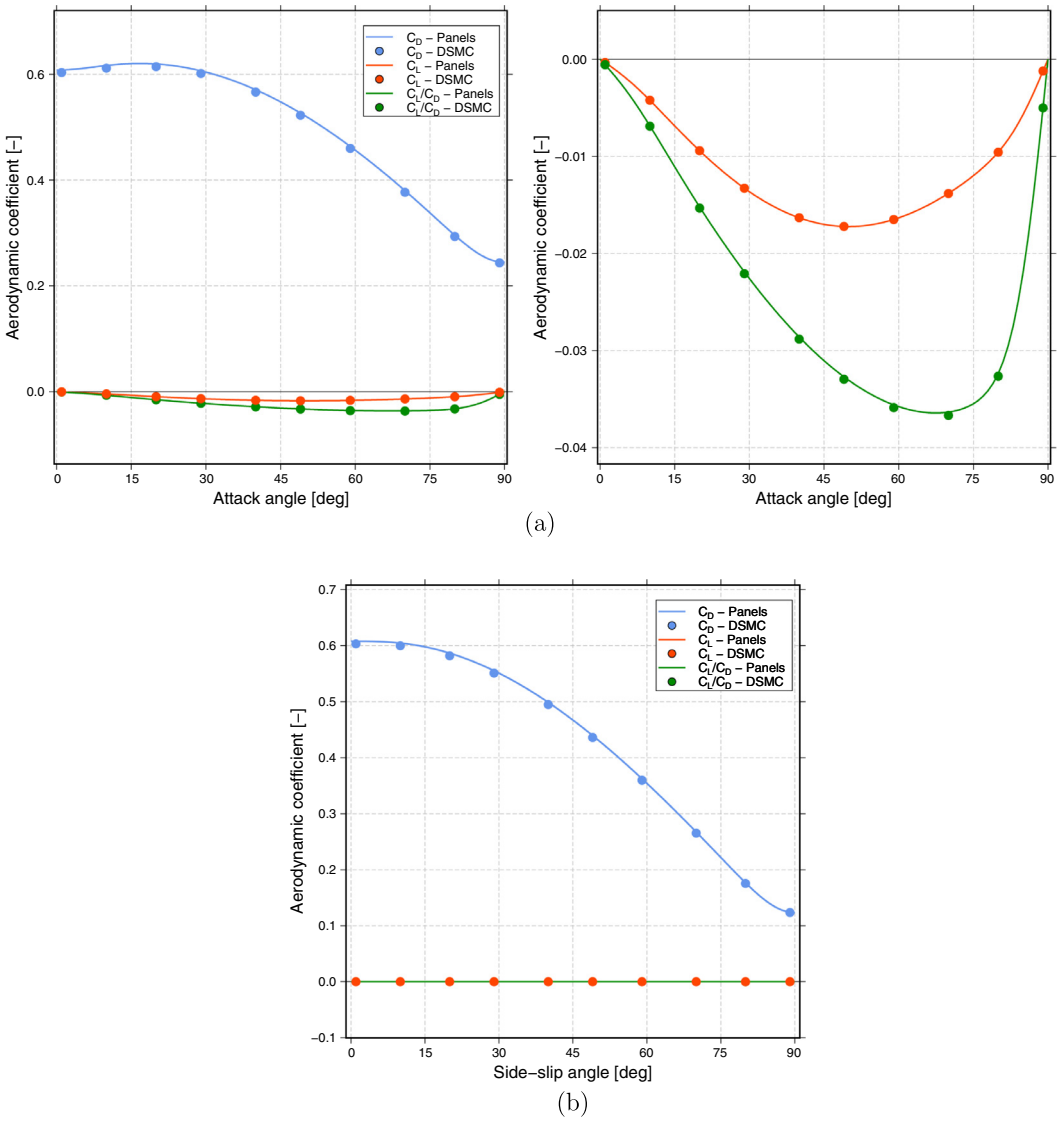

Fig. 4. SPARTA validation for a attack angle (a) and side-slip (b) rotations of a box. Aerodynamic coefficients for panel method (solid lines) are compared with DSMC computations (markers).

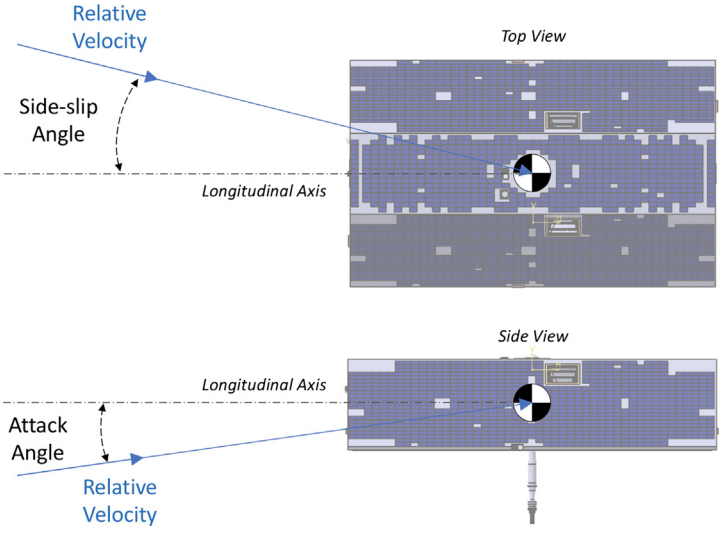

Fig. 5. Representation of side-slip and attack angles for GRACE.

aerodynamic coefficients for side-slip angle variations. For these figures, the left plot contains all quantities of interest (drag, lift and lift over drag ratio), whereas, the right plots offer a detailed description of exclusively lift and lift over drag ratio, which are characterised by lower values. The selected aerodynamic coefficients have been normalised with a reference area set to 1 m^2 for all missions. This reference area does not depend on the attack and side-slip angles, and therefore variations of the true flow-exposed area of the satellites do not need to be independently calculated. These are already captured in the normalised force coefficients which are a function of these angles. The normalised force coefficients shown in Figs. 6–13 were calculated with a speed ratio corresponding to 100% atomic oxygen and a temperature of 400 K. In order to process the new densities, the drag coefficients need to be computed for all the atmospheric constituents and summed to obtain the on-track values (Doornbos, 2011). Temperatures and

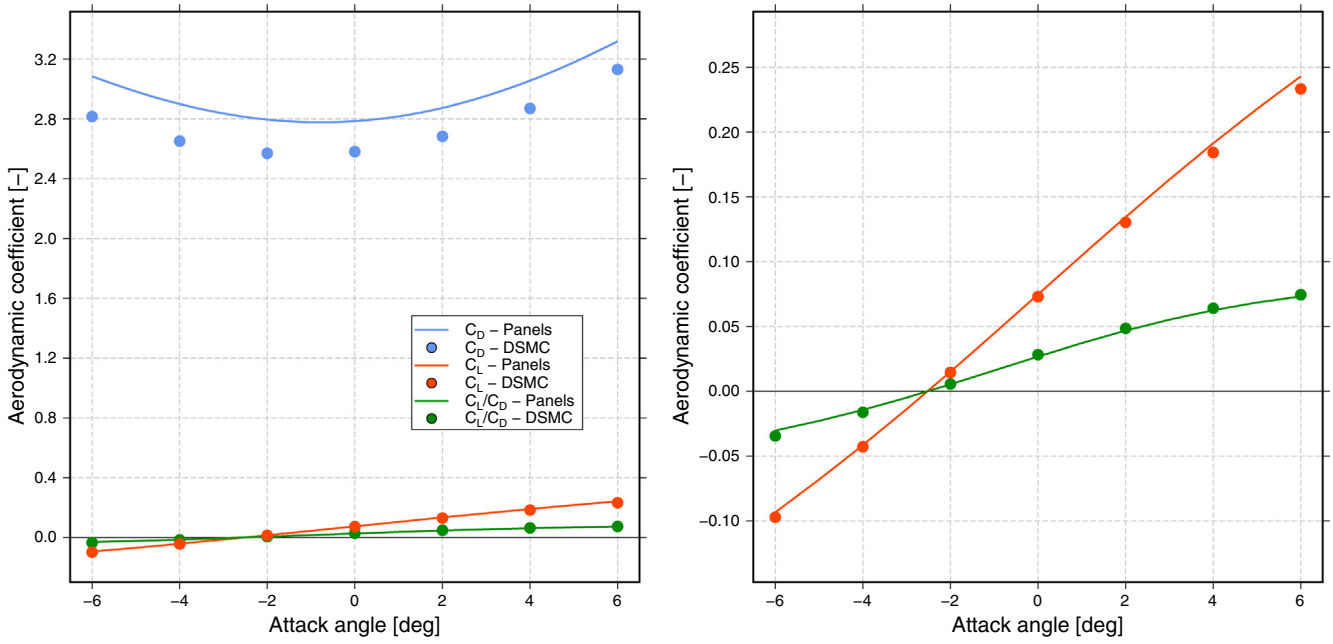

Fig. 6. Comparison between panel and SPARTA aerodynamic coefficients as a function of attack angles for CHAMP.

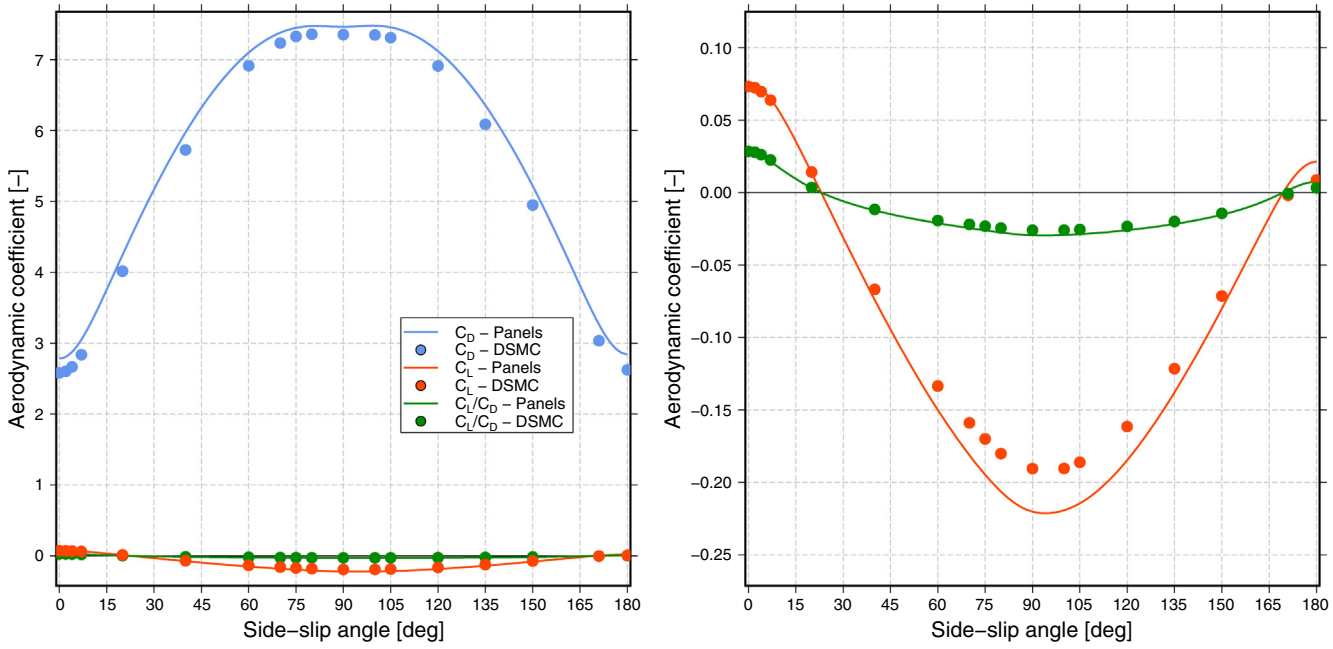

Fig. 7. Comparison between panel and SPARTA aerodynamic coefficients as a function of side-slip angles for CHAMP.

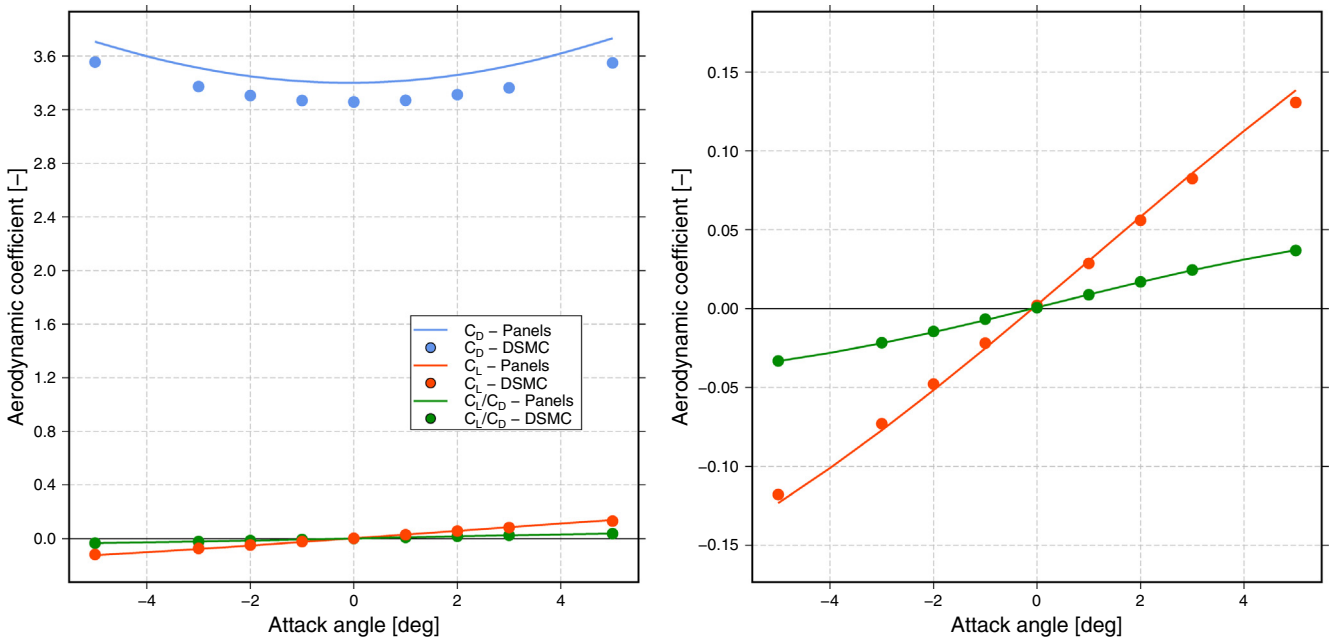

Fig. 8. Comparison between panel and SPARTA aerodynamic coefficients as a function of attack angles for GRACE.

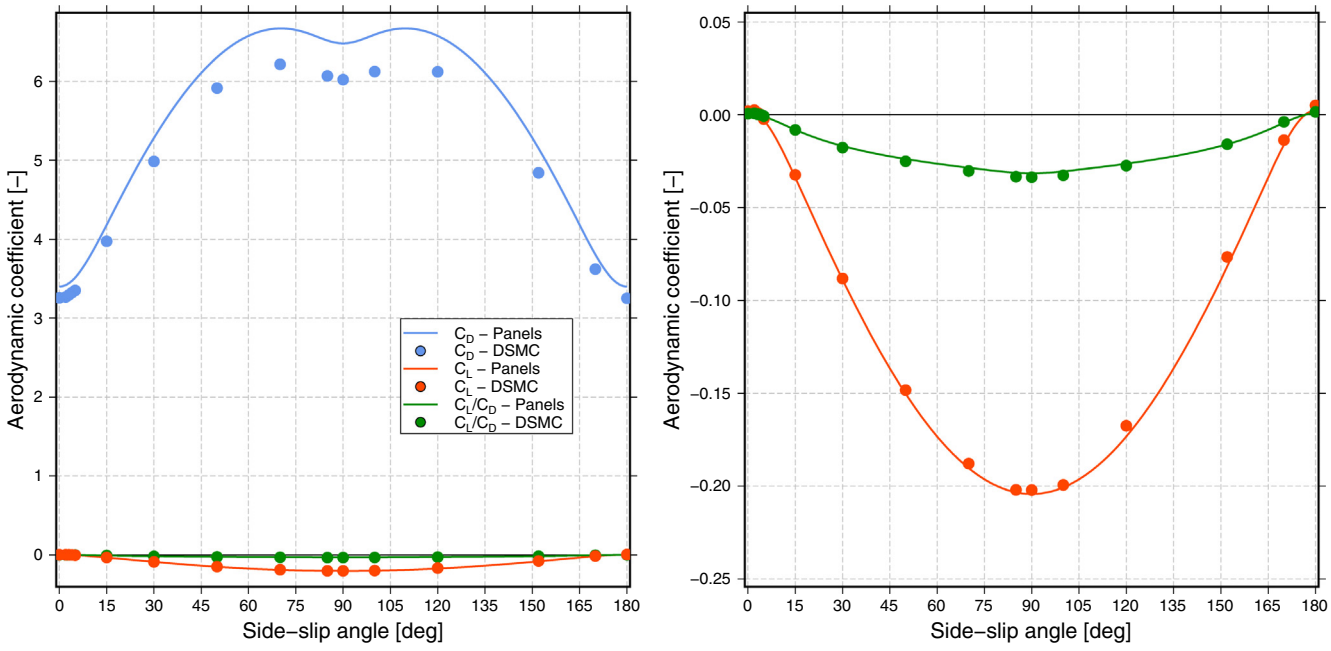

Fig. 9. Comparison between panel and SPARTA aerodynamic coefficients as a function of side-slip angles for GRACE.

the relative mass concentrations of atmospheric constituents depend on satellite locations and play a crucial role in the final density estimation. Introducing the results for the other satellites, Figs. 8 and 9 are for GRACE, Figs. 10 and 11 for GOCE and finally Figs. 12 and 13 for Swarm. Aerodynamic coefficients are available on the vertical axis, whereas selected attitude angles are on the horizontal axis. The drag coefficient is the predominant coefficient and analysing each satellite, it can be observed that coefficient differences are up to 32%. These discrepancies between panel and SPARTA methods are not constant between different satellites and turned out to be strictly related to satellite outer surface complexity. Indeed, the best agreement can be found for GRACE, which in comparison with other satellites is characterized by a simpler shape. Large differences are obtained for Swarm, while the differences are at a similar intermediate level for CHAMP and GOCE.

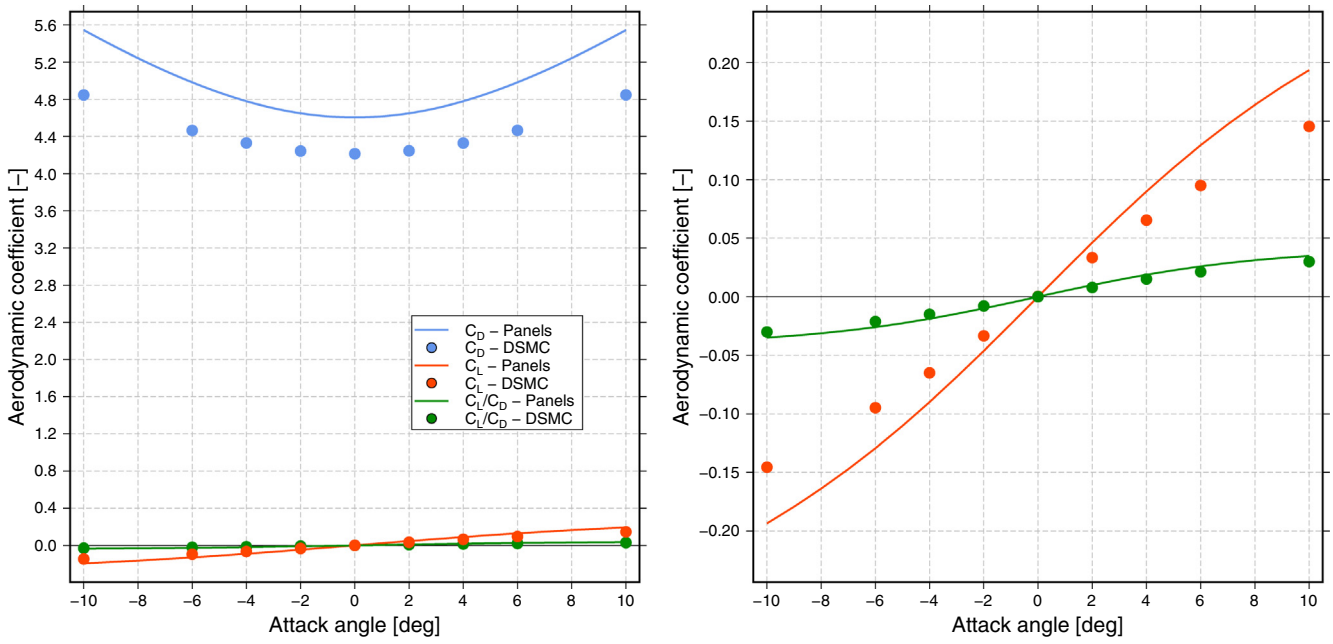

Fig. 10. Comparison between panel and SPARTA aerodynamic coefficients as a function of attack angles for GOCE.

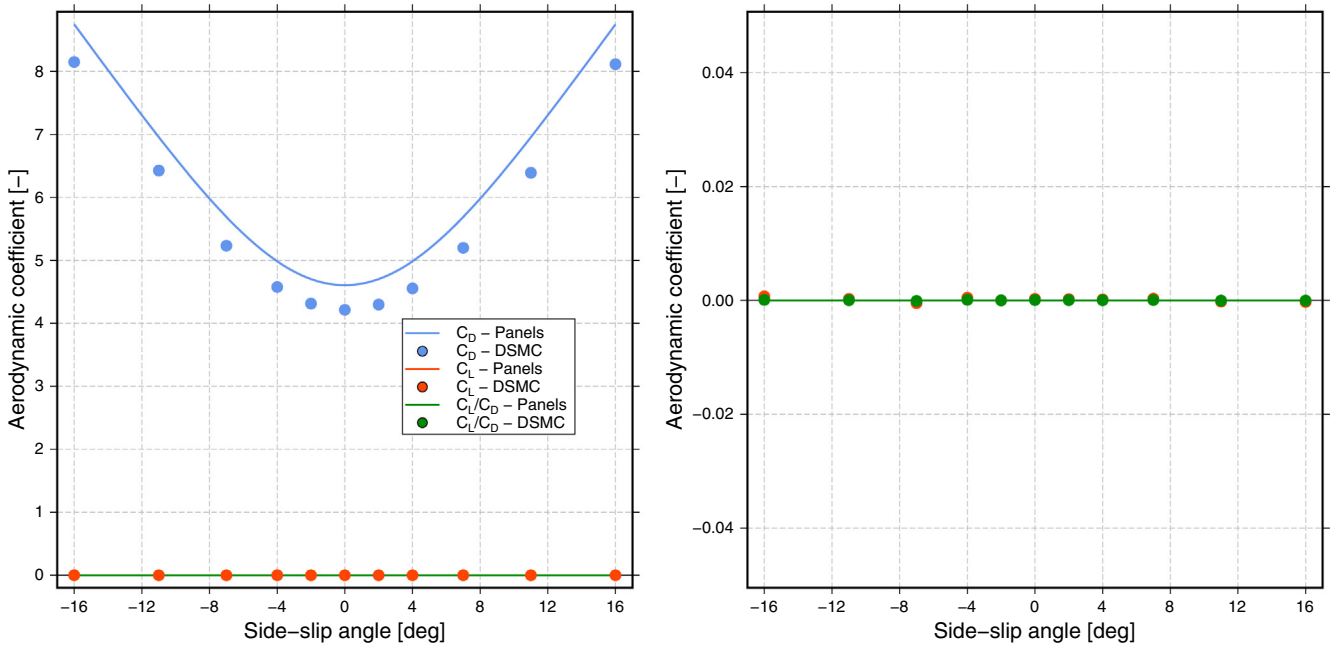

Fig. 11. Comparison between panel and SPARTA aerodynamic coefficients as a function of side-slip angles for GOCE.

The previous results have been obtained for a fixed speed ratio equal to 7. However a full range of different speed ratios between 1 and 14 has been analysed for each satellite. Low speed ratios occur at low molecular mass of the gas, and at high gas temperature. Whereas, high speed ratios are characterized by the opposite trends according to Eq. (9). Fig. 14 shows the evolution of drag coefficients depending on different speed ratios and selected side-slip angles.

From Fig. 14, it is possible to have a complete overview of the drag for the selected satellites and different speed ratios. It turns out that nominal flight configuration ($\beta = 0$) always provide overestimated drag coefficients from the panel method with respect to the DSMC approach. As shown before, for the CHAMP, GRACE, and GOCE satellites, the drag difference turns out to be less significant compared to Swarm. However, from these diagrams, it is clear that there are different behaviours also

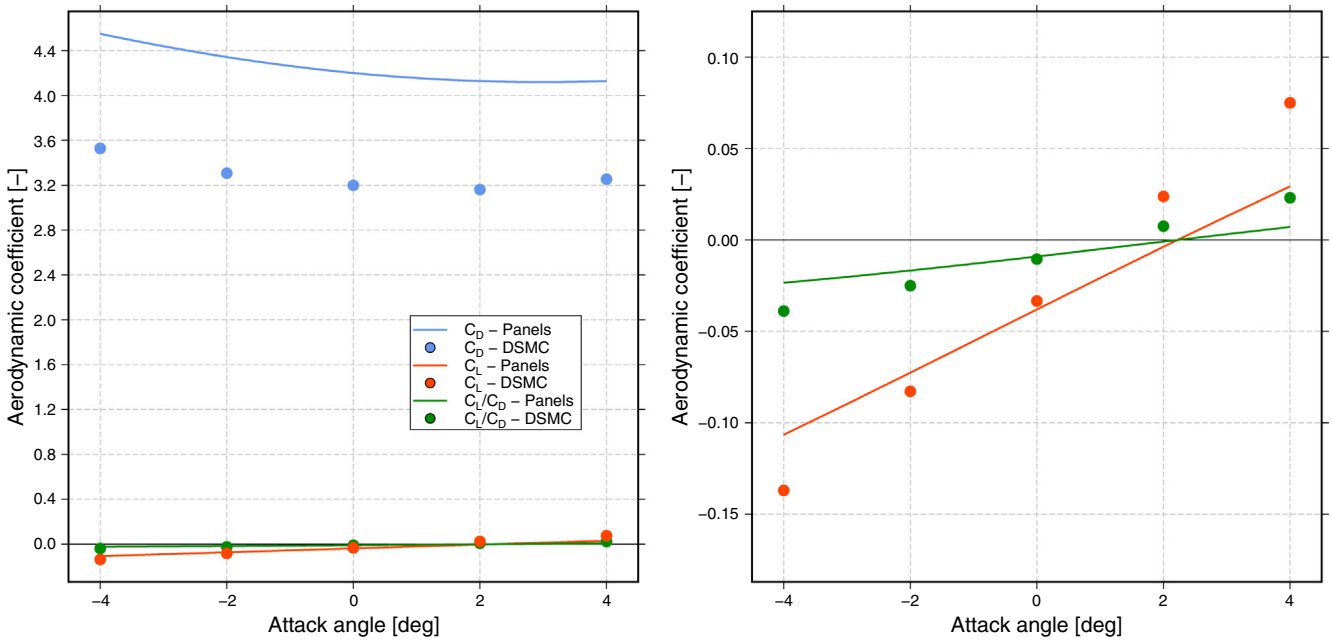

Fig. 12. Comparison between panel and SPARTA aerodynamic coefficients as a function of attack angles for Swarm.

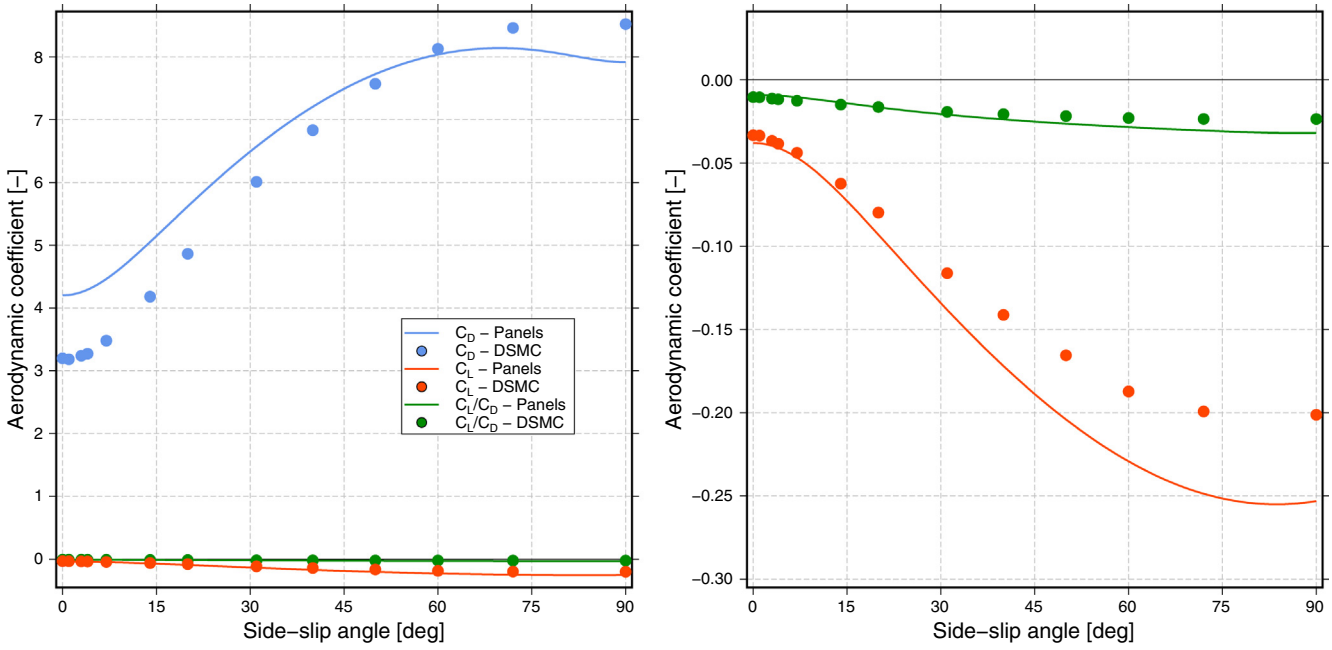

Fig. 13. Comparison between panel and SPARTA aerodynamic coefficients as a function of side-slip angles for Swarm.

for different side-slip angles. The panel method is not constantly overestimating or underestimating the drag, but the difference depends on the attitude and speed ratio. For the same satellite and side-slip angle, it is possible to find a better agreement or a larger discrepancy depending on the value of the speed ratio. This makes it necessary to have a complete and detailed description of satellite aerodynamics as a function of each of these inputs encountered during the mission lifetime. An accurate description about the orbit is obtained from the star camera attitude data. Whereas, the information about the atmospheric composition to model the speed ratio along the orbit is provided by the NRLMSISE-00 model (Picone et al., 2001). A complete and detailed aerodynamic data set is generated from these outputs and these preliminary results are used as input for the density processing explained in the next section.

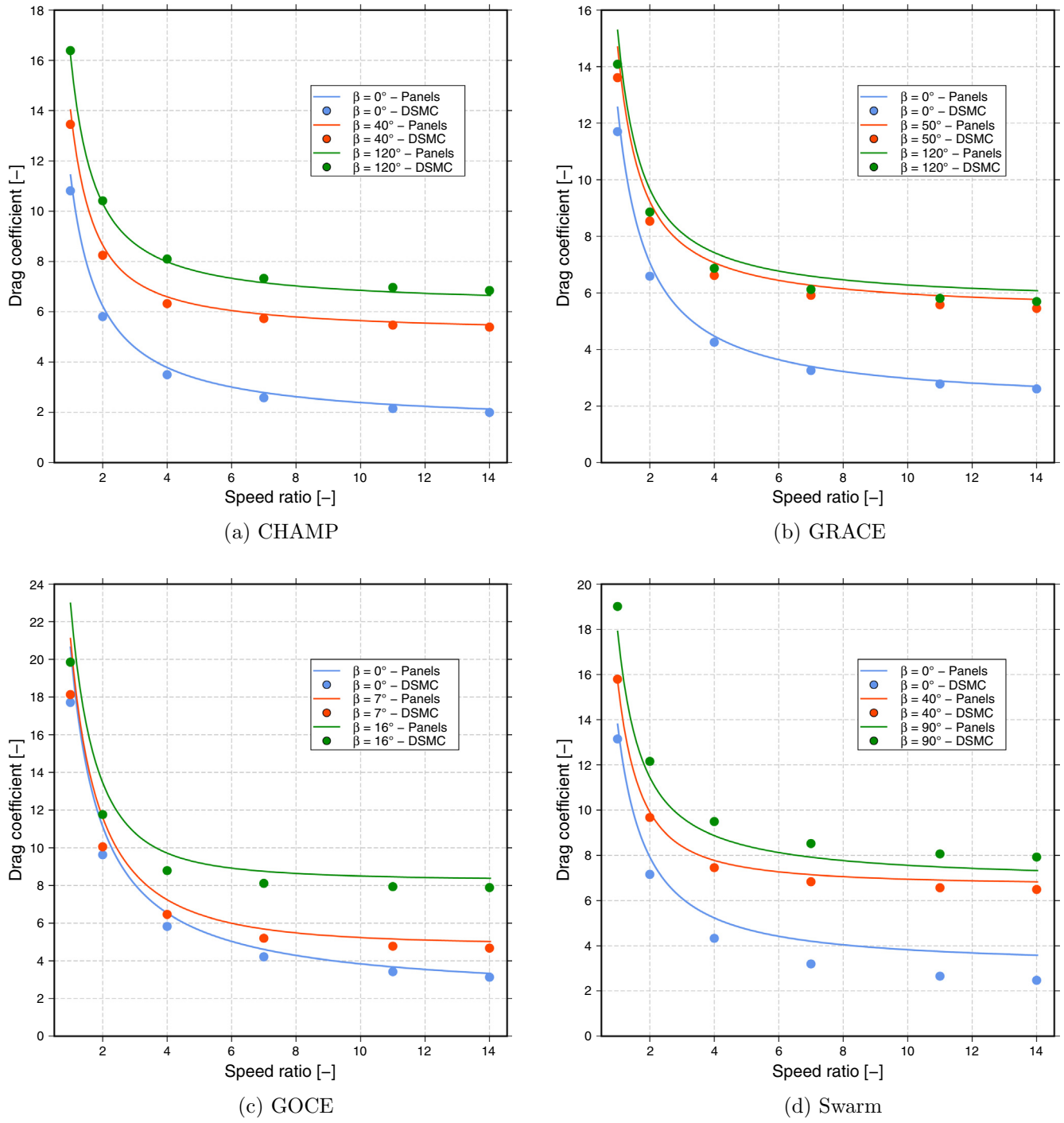

Fig. 14. Drag coefficients as a function of the speed ratio for selected side-slip angles.

5. Density processing

Processing accelerations introduces the use of three orthogonal acceleration observations and four unknowns which are the density and the three wind velocity components. The satellite relative velocity is provided by the combination of orbit, co-rotation and wind velocities. The first two are known with higher fidelity with respect to the winds, which can be obtained from specific models. Raw accelerometer data need to be processed to remove various non-aerodynamic accelerations. These are mostly due to radiation pressure, thrusters and mechanical forces from electrical currents (Flury et al., 2008). The density is one of the scientific results obtainable from accelerations. As mentioned in the introduction, many studies have been published on this processing. Among recent scientific

papers, Pilinski et al. (2016) and Mehta et al. (2017) provided improved aerodynamic modelling for the DANDE, POPACS (Pilinski et al., 2016), CHAMP and GRACE (Mehta et al., 2017) satellites. In Pilinski et al. (2016), the main attention is focused on the aerodynamics of two satellites independently of the atmospheric density. Similar computations (as explained in Section 4) are used and a comparison with closed-form solutions is also available. Simpler satellite shapes like DANDE allow for a direct comparison with analytical solutions. However, the geometric complexity of the selected satellites of this work does not allow a direct comparison with a single closed-form solution, but only with a sum of multiple contributions from flat panels. As mentioned in the introduction, both papers use the TPMC technique. In particular, Mehta et al. (2017) simulations are based on new geometries, which are designed with a CAD software. Unlike this paper, Mehta et al. (2017) assumes zero atmospheric winds. The absence of atmospheric winds introduces uncertainties between 5% and 20% on estimated densities (Sutton, 2008). Large uncertainties are especially detected for high latitudes and geomagnetic active conditions. In the current paper, atmospheric winds are computed with atmospheric models (i.e. HWM07), and where possible, wind components can be derived from the acceleration data. Wind models are based on large amounts of observations, the uncertainties are usually based on the natural variability of the system and the observational uncertainties which can reach values greater than 100 m/s (Drob et al., 2008, 2015).

Both Pilinski et al. (2016) and Mehta et al. (2017) use variable gas-surface interactions (GSI) models. These models provide different behaviours with respect to fully diffusive reflections and are applicable to the presented geometries. However, a further development of current GSI models is necessary. Exploiting multiple satellite data sets as well as analysing lift, torques, in addition to drag, would potentially allow an optimization of GSI parameters, which will help to obtain more consistent density data. This is based on a first crucial step that consists of a high-fidelity geometry modelling, which is fully characterized in this work.

The densities from Sutton (2008) and Mehta et al. (2017) have been retrieved from the supplemental data from Mehta et al. (2017). In this section, a comparison for the three representative days selected in Mehta et al. (2017) is performed with the new densities presented in this paper. An additional comparison with Sutton results is also included. The analysed days are: 2002-10-27, 2005-05-15 and 2009-08-28. The day in 2002 is associated to high solar activity, whereas the 2005 and 2009 days are respectively for moderate and low activities. This comparison covers the data of the CHAMP and GRACE satellites. Full statistical details for the complete days are provided in Table 4. Whereas, Figs. 15, 17 and 18 show the comparison between SPARTA, Mehta et al. (2017),Sutton (2008) and Doornbos (2011) estimated densities for the CHAMP satellite within the first three hours of each day. Figs. 19–21 show the same comparison for the GRACE satellite. In each Figure, a direct comparison between densities is available in the top plot. The second plot presents the ratio between external and SPARTA densities. Only for the CHAMP satellite, a full day plot is available in Fig. 16 to highlight a lack of data among the data sets. The flagged area in grey associated to a lack of accelerations is due to missing star camera attitude data. This interval ranges between 18:32-19:20 UTC. This gap was linearly interpolated in Fig. 3 of Mehta et al. (2017). In Table 4 the flagged data are excluded from statistical comparisons. All the other days, including those ones for GRACE, do not have additional flags. In Table 4, the mean difference (MD) and mean ratio (MR) are computed as

$$MD = mean\left(\frac{|\rho_{ext} - \rho_{spa}|}{\rho_{spa}} \cdot 100\right)$$
$$MR = mean\left(\frac{\rho_{ext}}{\rho_{spa}}\right) \tag{10}$$

Table 4
Comparison of SPARTA results with Mehta et al. (2017) [M] Sutton (2008) [S] and Doornbos (2011) [D] estimated densities

Satellite		Source	27-10-2002	15-05-2005	28-08-2009
CHAMP	Mean Diff. [%]	M	5.27	3.92	5.41
		S	12.92	15.84	16.15
		D	6.03	5.84	6.09
	Mean Ratio [–]	M	0.96	0.97	0.95
		S	1.12	1.16	1.16
		D	0.94	0.94	0.94
GRACE	Mean Diff. [%]	M	17.38	22.84	23.93
		S	7.05	8.67	17.65
		D	3.39	3.44	4.67
	Mean Ratio [–]	M	0.83	0.77	0.83
		S	0.93	0.92	1.08
		D	0.97	0.97	0.95

The ρ_{ext} is the density estimated by one of the external sources, whereas ρ_{spa} is the density obtained from SPARTA simulations. The comparison for CHAMP shows a higher agreement with the results from Mehta and Doornbos. However, for Sutton's data set, the differences are larger. The new results match well with Doornbos' previous data for both missions. The density ratios based on Doornbos' data in Figs. 15–21 have a smoother behaviour compared to the other two data sets, especially for GRACE. Indeed, a nearly constant density ratio can be found in Figs. 19–21. Analogous trends are obtained comparing independently Sutton and Mehta results. This might be related to a similar accelerometer calibration processing between Sutton-Mehta results from one side and Doornbos-SPARTA results from the other. For example, for the GRACE satellite, the presence of spikes in the SPARTA-Doornbos results are associated to attitude thruster effects. These disturbances in the accelerations have been differently filtered out in the other two sets. This creates a double similarity and discrepancy respectively within and between the two couples of sets. Differences in dealing with additional acceleration contributions, such as solar radiation pressure, can create further variations between the analysed sets.

For CHAMP, Table 4 shows a higher agreement between SPARTA and Mehta et al. (2017) with respect to Doornbos (2011) and Sutton (2008). Indeed, among the three representative days, there is an average percentage

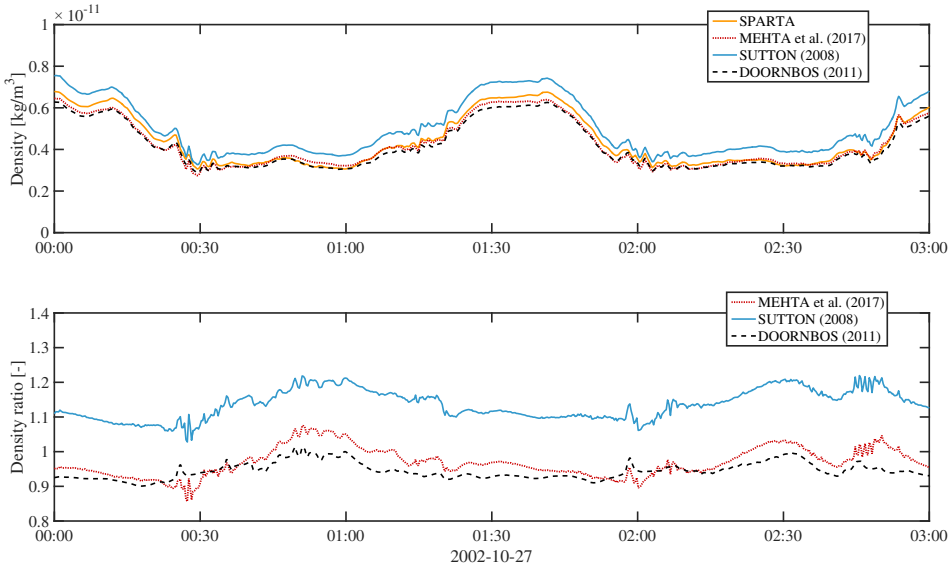

Fig. 15. Comparison of SPARTA results with Sutton (2008),Mehta et al. (2017) and Doornbos (2011) CHAMP density data sets on the first 3 h of 2002-10-27.

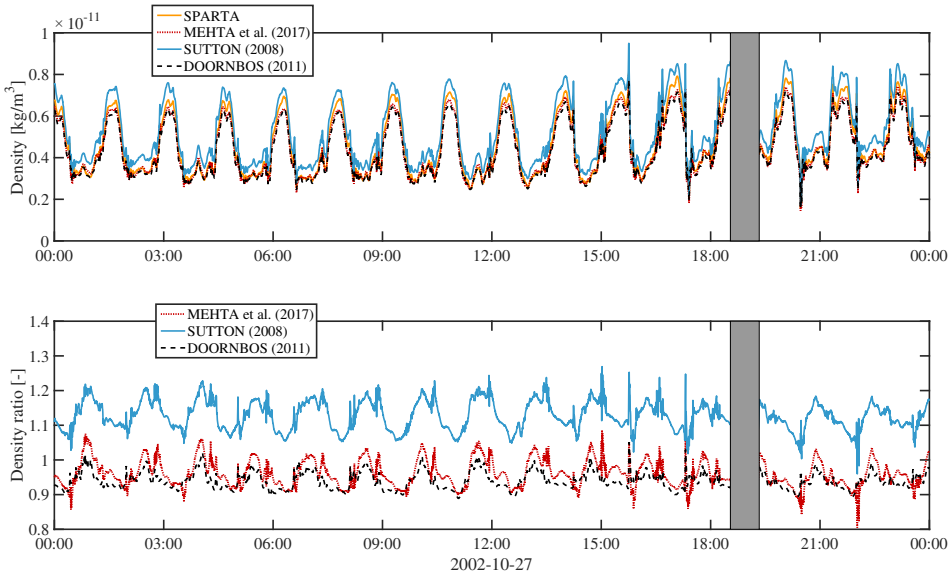

Fig. 16. Comparison of SPARTA results with Sutton (2008),Mehta et al. (2017) and Doornbos (2011) CHAMP density data sets on 2002-10-27. The grey area is associated to a lack of star camera attitude data (18:32-19:20 UTC).

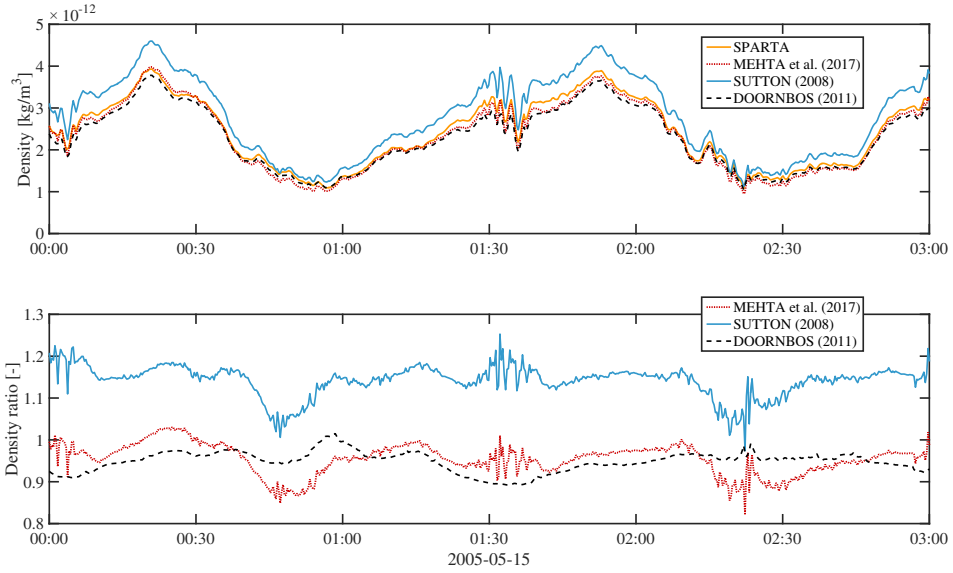

Fig. 17. Comparison of SPARTA results Sutton (2008),Mehta et al. (2017) and Doornbos (2011) CHAMP density data sets on the first 3 h of 2005-05-15.

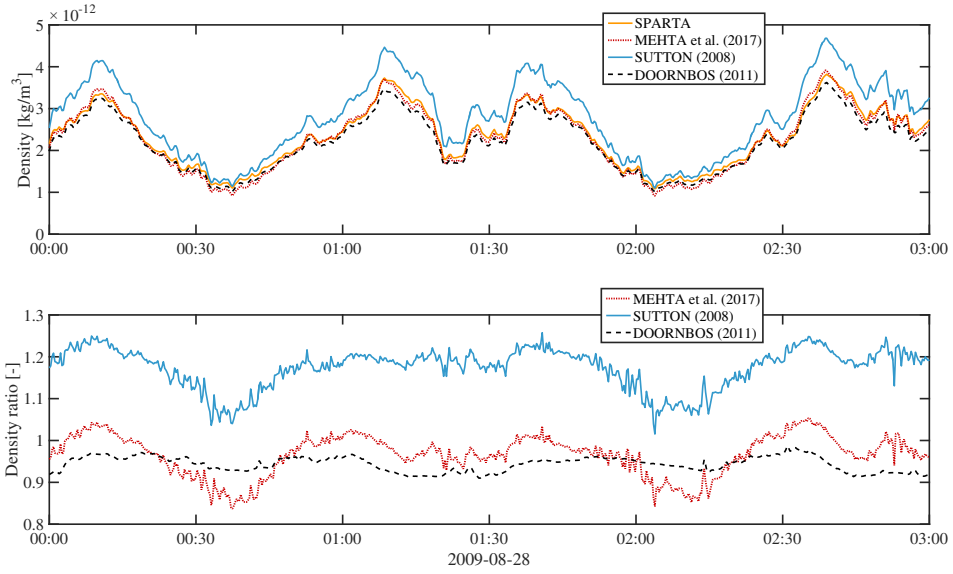

Fig. 18. Comparison of SPARTA results Sutton (2008),Mehta et al. (2017) and Doornbos (2011) CHAMP density data sets on the first 3 h of 2009-08-28.

difference of 4.9% with Mehta et al. (2017), 6% with Doornbos (2011) and 15% with Sutton (2008). Whereas, for GRACE, the agreement with Doornbos (2011) is better. Calculated average differences are 21.4% with Mehta et al. (2017), 11.1% with Sutton (2008) and 3.8% with Doornbos (2011). Differences within the three representative days are similar. However, densities estimated by Sutton turned out to be highly correlated with SPARTA results for high solar activity. This result can be associated to the different assumptions on the gas-surface interaction. Indeed, Sutton (2008) used a constant value of 0.93 for the energy accommodation coefficient, which is in agreement with high solar activities (Mehta et al., 2013). From the other side, for Mehta et al. (2017), a Cercignani-Lampis-Lord (CLL) model is used (Walker et al., 2014) and the comparison shows a more constant behaviour for differences. The adoption of lower accommodation coefficients leads to higher drag coefficients, which result in lower densities. Therefore, further research on GSI can reduce current discrepancies with Mehta et al. (2017).

In the following Sections 5.1 and 5.2, the results concerning density processing are provided through two different studies. The first relies on statistical comparisons between panel and SPARTA method for long time periods. The second one is focused on specific yaw-manoeuvres in short time windows.

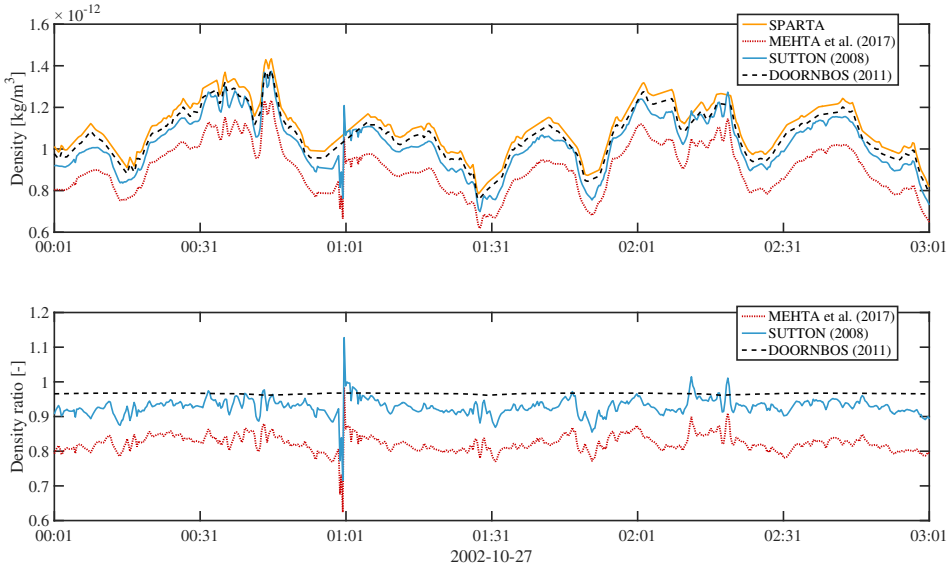

Fig. 19. Comparison of SPARTA results with Sutton (2008),Mehta et al. (2017) and Doornbos (2011) GRACE density data sets on the first 3 h of 2002-10-27.

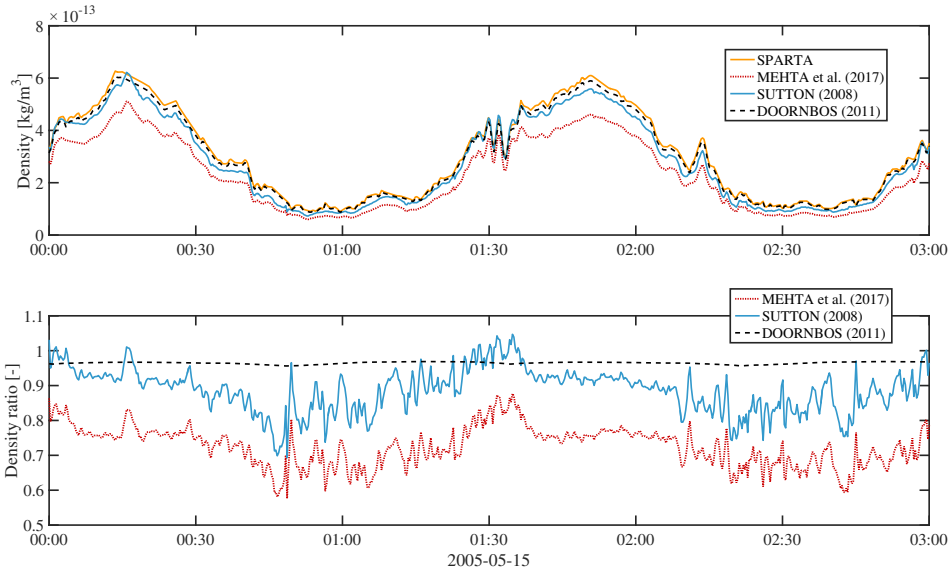

Fig. 20. Comparison of SPARTA results Sutton (2008),Mehta et al. (2017) and Doornbos (2011) GRACE density data sets on the first 3 h of 2005-05-15.

5.1. Comparison with semi-empirical models

In order to process data, the Direct and the Iterative algorithms from Doornbos (2011) have been adapted to SPARTA and applied to the complete set of CHAMP, GRACE, GOCE and Swarm satellites. Using these algorithms, panel method output can be directly compared with new aerodynamic datasets from SPARTA. Taking into account nominal flight conditions for long periods, it is possible to retrieve statistical information about densities in comparison with available atmospheric models. These comparisons have been performed for both panel and SPARTA methods. The reference frame is chosen with X direction along the track, Y along cross-track and Z along radial orientation. For a nominal flight configuration, Euler angles are small and the inertial satellite velocity is mostly aligned with the satellite longitudinal axis. In this case, it is possible to take into consideration only the X-component of the accelerations. This procedure is used within the Direct algorithm for density processing discussed in Sutton (2008) and Doornbos et al. (2010). All four selected missions have been investigated. Swarm-A and -C provided the same results because of their similar orbit and for this reason, they are listed together. For GRACE, only new densities from GRACE-A are shown because the twin satellite (GRACE-B) provided the same results. Fig. 23 presents a comparison of thermospheric densities for Swarm Charlie with the two different geometry

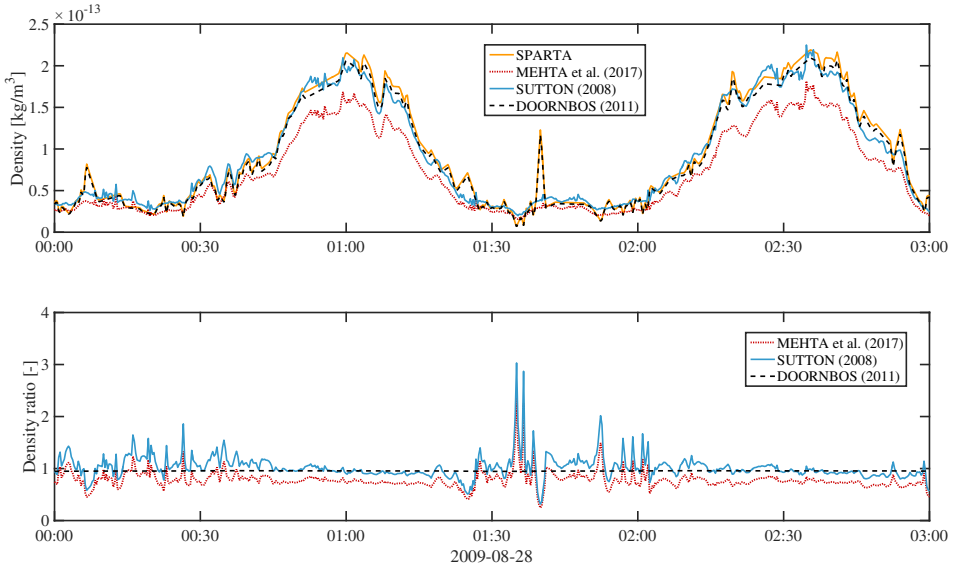

Fig. 21. Comparison of SPARTA results Sutton (2008),Mehta et al. (2017) and Doornbos (2011) GRACE density data sets on the first 3 h of 2009-08-28.

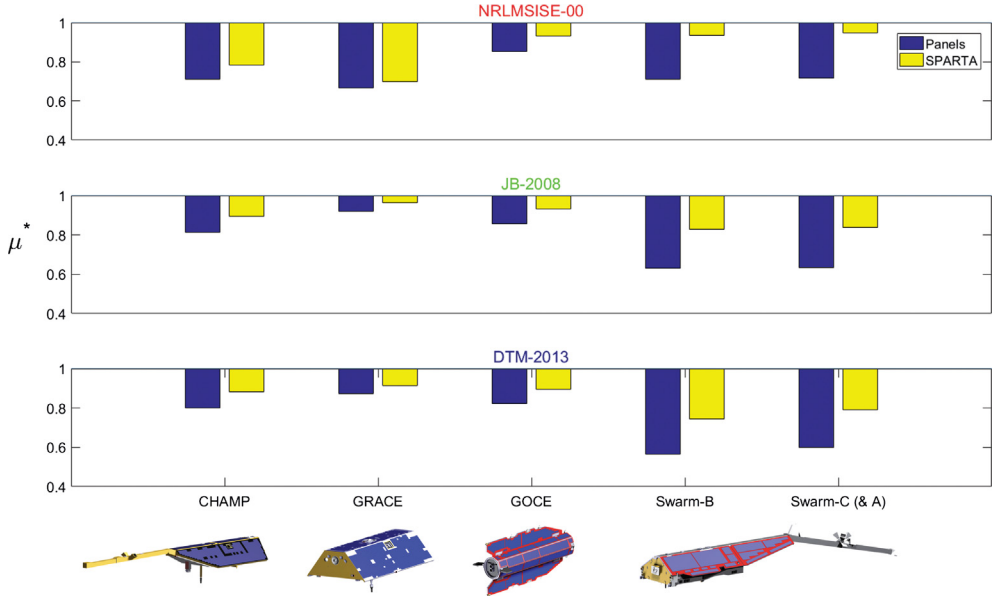

Fig. 22. Comparison between panel and SPARTA densities for CHAMP, GRACE, GOCE and Swarm.

modellings. In this figure, SPARTA and panel method results are compared with NRLMSISE-00 atmospheric model (Picone et al., 2001). The statistical results are presented in the top left part of each diagram by two parameters. These values are the log-normal mean ratio of estimated densities over atmospheric model densities (μ^*) and the log-normal standard deviation (σ^*). Densities are estimated in the period between 2014-07-19 and 2016-09-30. For this particular density model, the mean ratio shows a significantly better agreement. The standard deviation is nearly constant. This is associated to the same difficulty in modelling additional contributions like solar radiation pressure. Looking at low densities, the data cloud turns out to be wider. Indeed, lower densities are characterized by lower aerodynamic contribution to the total acceleration which reaches radiation pressure magnitudes. In these areas, solar radiation pressure incorrect modelling have more impact on densities. Further improvement of radiation pressure modelling would reduce errors in the measured densities. The achieved percentage differences for the set of satellites depends on the reliability of previous panel geometry modellings, which turns out to have been more accurate for simpler satellite geometries. For GRACE, which is characterized by a simpler shape, the

improved densities registered a difference of +5%. Whereas, new geometry models for CHAMP and GOCE provided changes of 11% and 9% respectively. In all cases, the changes were towards better agreement with the models (Fig. 22). This study has been conducted also comparing with different atmospheric models (NRLMSISE-00, JB-2008 (Bowman et al., 2008) and DTM-2013 (Bruinsma, 2015)).

Investigated periods cover years of data in order to provide satisfactory statistical information. The longest periods between manoeuvres and the quality of satellite data have been analysed in order to provide a reliable statistical information. In particular, the analysed periods range between 2002-11-07 and 2008-12-31 for CHAMP, 2005-12-12 and 2009-03-17 for GRACE, 2009-11-01 and 2013-11-05 for GOCE and, as mentioned before, 2014-07-19 and 2016-09-30 for Swarm satellites. For all the comparisons, an improvement in the agreement with atmospheric models is achieved. An overview of obtained results is available in Table 5.

Depending on the mission and atmospheric model, average mean ratios change. New Swarm densities turned out to be better correlated with the NRLMSISE-00 model. However, CHAMP and GRACE are in better agreement with JB-2008. GOCE satellite densities are performing nearly equally for both NRLMSISE-00 and JB-2008. The results of this analysis provided scale factors which can be applied to previous panel method output to have a fast improvement of current densities. This is a reliable approach in case of nominal flight configurations. However, in the presence of manoeuvres or prolonged attitude changes, the provided factors are not applicable. For what concerns the Swarm mission, the presented results are currently adopted for Swarm L2 data product processing of the DNSxPOD products (Doornbos et al., 2017).

Table 5
Comparison of SPARTA results with NRLMSISE-00, JB-2008 and DTM-2013 atmospheric models

Satellite	μ^*-panel	μ^*-SPARTA	σ^*
NRLMSISE-00			
CHAMP	0.712	0.785	1.27
GRACE	0.668	0.699	1.42
GOCE	0.854	0.931	1.18
Swarm B	0.711	0.935	1.46
Swarm C (& A)	0.717	0.949	1.29
JB-2008			
CHAMP	0.813	0.896	1.22
GRACE	0.920	0.964	1.44
GOCE	0.856	0.933	1.16
Swarm B	0.630	0.828	1.42
Swarm C (& A)	0.633	0.837	1.24
DTM-2013			
CHAMP	0.800	0.882	1.22
GRACE	0.874	0.915	1.38
GOCE	0.823	0.896	1.16
Swarm B	0.566	0.745	1.41
Swarm C (& A)	0.598	0.791	1.24

5.2. Attitude manoeuvres analysis

In this section, the presented geometry models cover additional attitude configurations demonstrating that high fidelity densities can be provided also within manoeuvres. In order to estimate the new densities, it is necessary to use the iterative algorithm from Doornbos et al. (2010). Differently from the Direct algorithm, the relative velocity vector is not assumed to be aligned with the X axis of the satellite body frame, but it is adjusted to the realistic direction resulting in a match between directions of observed and modelled accelerations. After the adjustment in direction, it is necessary to match the magnitude of the

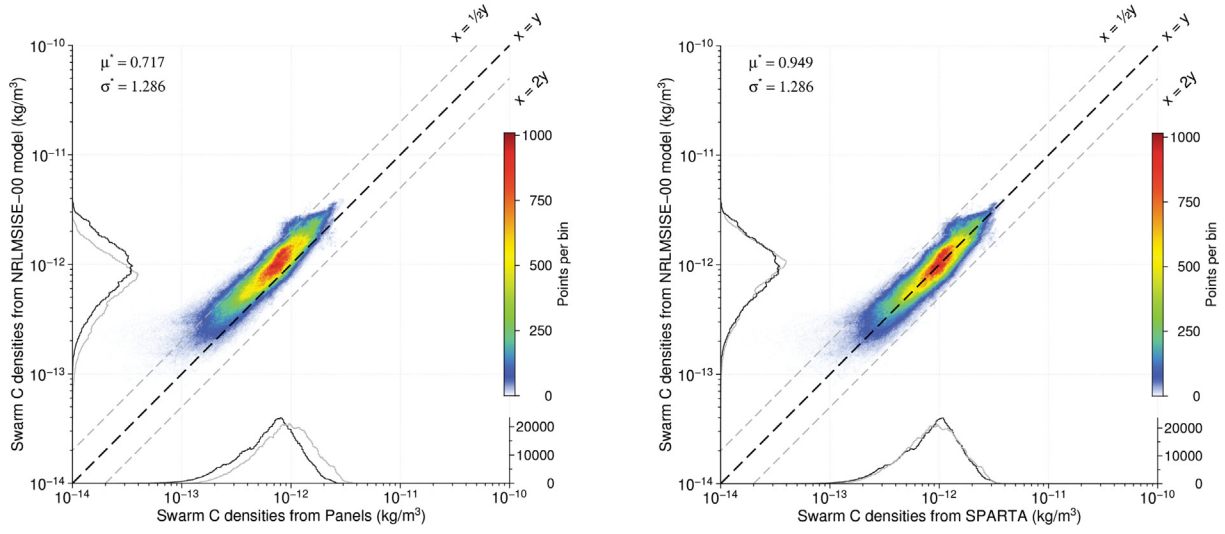

Fig. 23. Diagrams showing the distribution of Swarm C density data with equivalent NRLMSISE-00 model output. The colour scale indicates the number of points per bin. Panel method densities (left) are compared with SPARTA results (right).

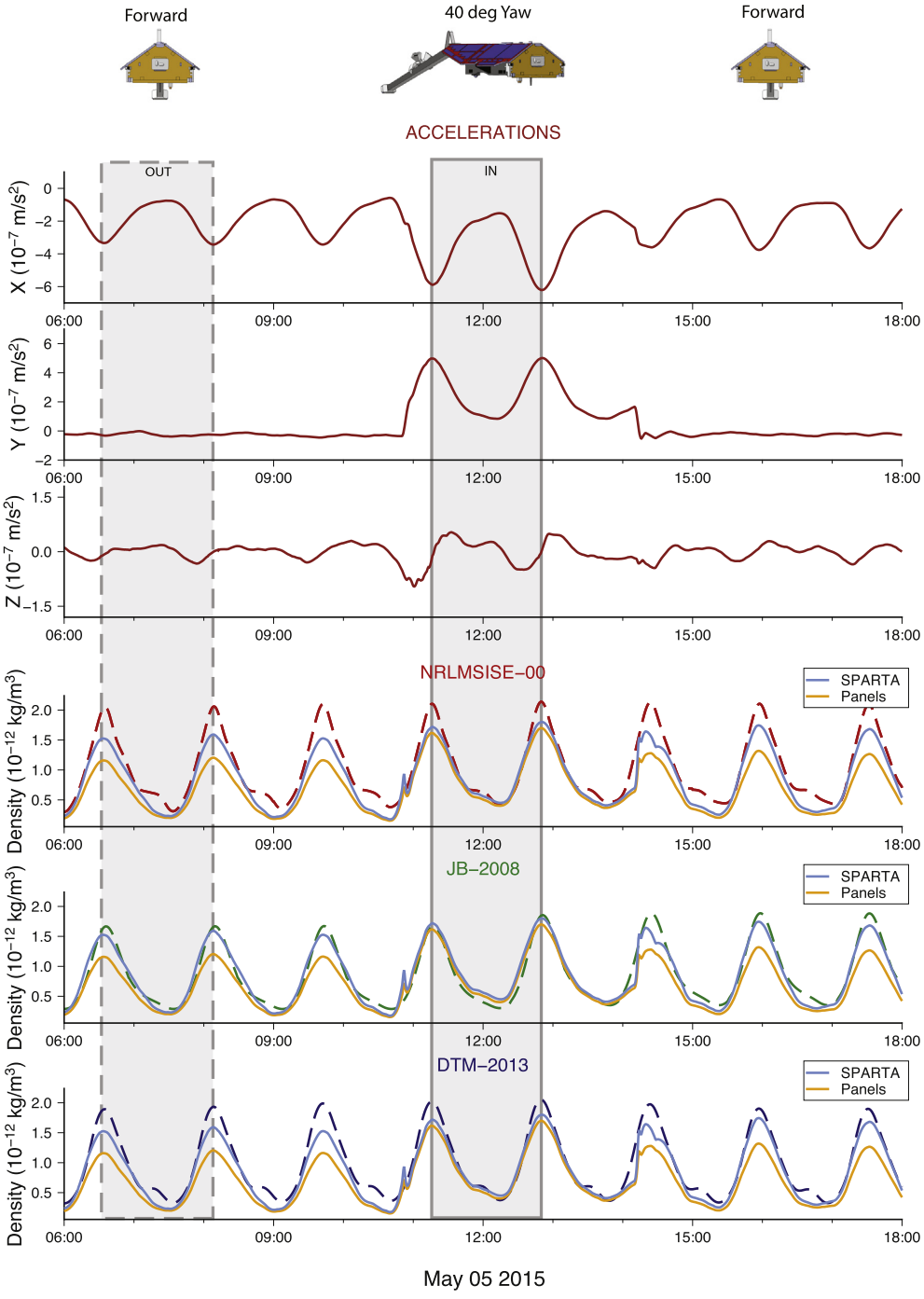

Fig. 24. Swarm-A densities for panel method and SPARTA during 40 deg yaw manoeuvre on 2015-05-05. Comparison with three atmospheric models: NRLMSISE-00, JB-2008 and DTM-2013.

acceleration to finally retrieve the density. After a few iterations, the density is modified in order to reach the final match and find the best fitting value. If the geometric and aerodynamic modelling would be reliable, the processed density remains nearly constant between the periods inside and outside the attitude manoeuvre. If the geometry is not accurately modelled, alterations in the density trends can be found. A perfect continuous match is not achievable because of the variability of the thermosphere. However, the densities are expected to stay approximately in the same range within a few orbits under stable geomagnetic activity conditions.

In this section, the results about densities within three attitude manoeuvres encountered within the CHAMP and Swarm missions are shown. The first manoeuvre is a 40 deg yaw-manoeuvre for Swarm-A. This change of attitude has been performed on the 5th of May 2015. The variation started at 10:50 UTC and was back to the nominal

state at 14:20 UTC. Fig. 24 includes a wider time domain (6:00–18:00 UTC), which shows the differences in accelerations and densities before, during and after the manoeuvre. Fig. 25 provides a similar plot. In this case, the performed manoeuvre is about 90 degrees. This is a combination of manoeuvres, four times the satellite changed its attitude by 90 degrees. Fig. 25 presents only a zoom-in within the first rotation. For both plots, panel method densities are characterized by large alterations between outside and inside the manoeuvre. However, for SPARTA a higher level of consistency is detected.

The side area is the predominant part for all these satellites and it is easier to model with respect to the frontal area, which is full of instruments protruding out of the main satellite body. For this reason, when the satellite is out of the nominal state, a better agreement between the

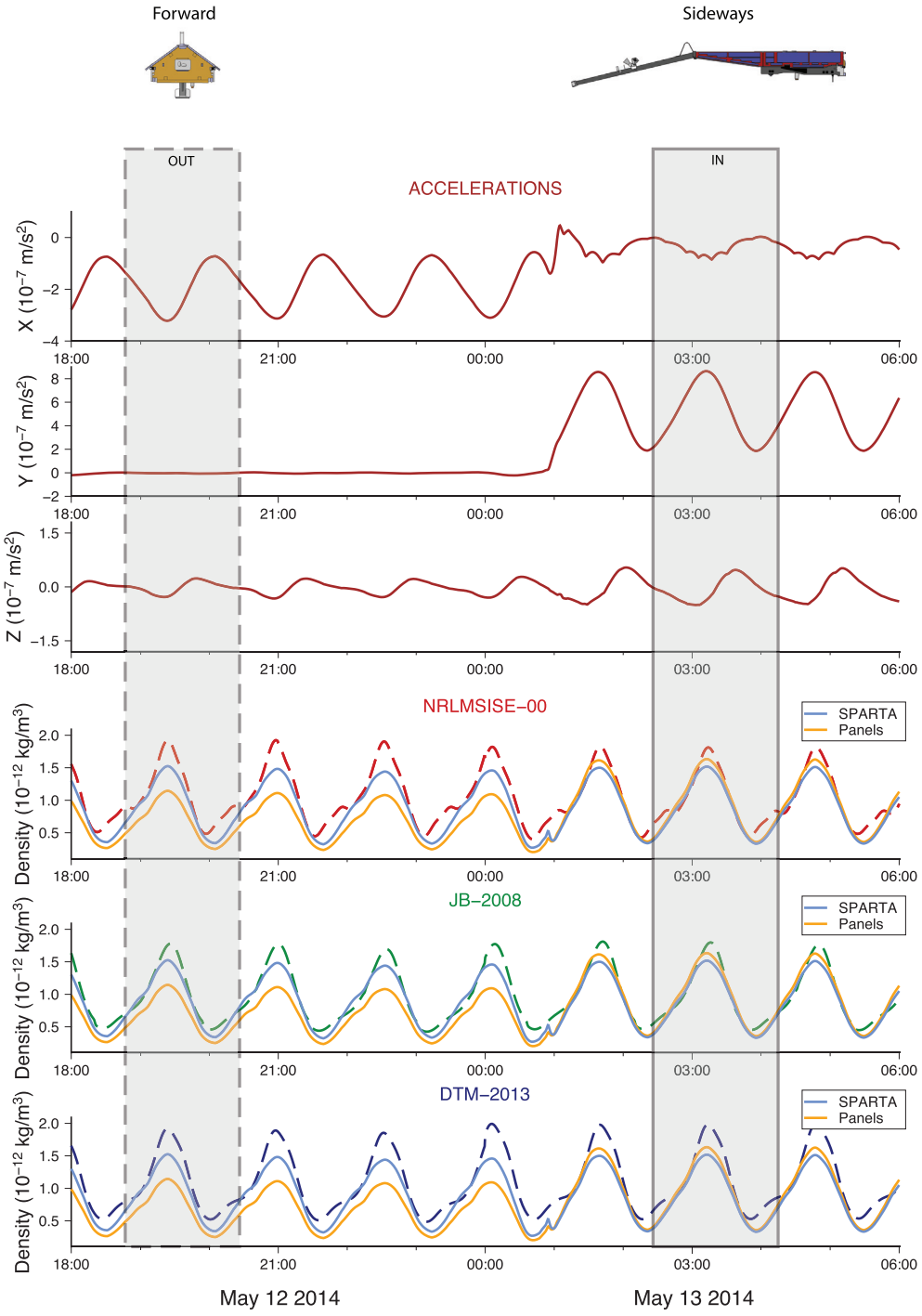

Fig. 25. Swarm-A densities for panel method and SPARTA during 90 deg yaw manoeuvre on 2014-05-13. Comparison with three atmospheric models: NRLMSISE-00, JB-2008 and DTM-2013.

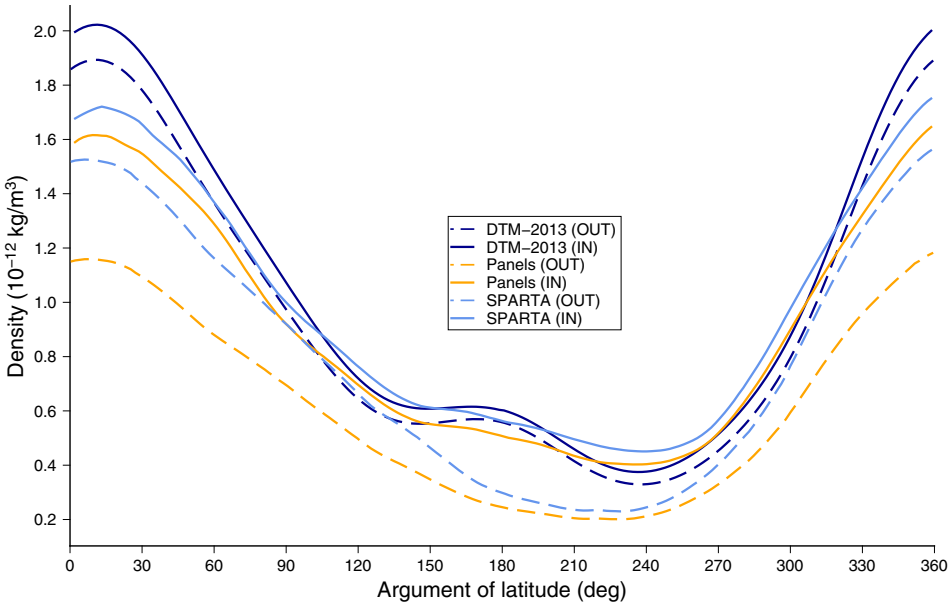

Fig. 26. Swarm-A densities for panel method and SPARTA during 40 deg yaw manoeuvre on 2015-05-06. Comparison with DTM-2013. The line types correspond to the data equally marked in Fig. 24 for outside (dashed) and inside (solid) the analysed attitude manoeuvre. Outside: 2015-05-05, 6:32:00-8:05:30 UTC. Inside: 2015-05-05, 11:13:30-12:46:30 UTC.

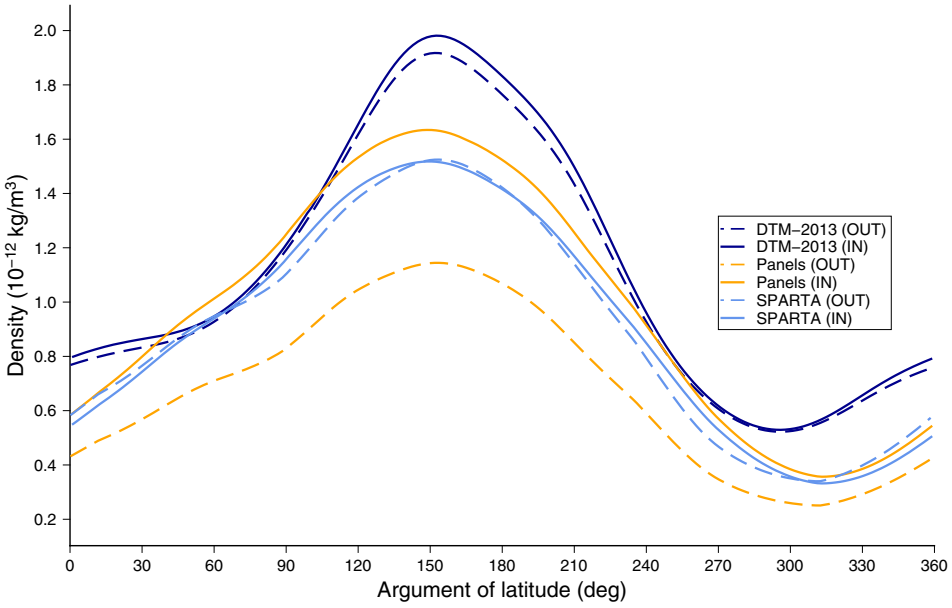

Fig. 27. Swarm-A densities for panel method and SPARTA during 90 deg yaw manoeuvre on 2014-05-13. Comparison with DTM-2013. The line types correspond to the data equally marked in Fig. 25 for outside (dashed) and inside (solid) the analysed attitude manoeuvre. Outside: 2014-05-12, 18:44:00-20:17:30 UTC. Inside: 2014-05-13, 2:34:00-4:07:30 UTC.

two models is reached. The panel method differently describes the two attitudes for both manoeuvres, whereas, a continuous consistency is detected for the SPARTA model. If the attention is focused within two orbits, outside and inside the presented manoeuvres (highlighted in grey areas in Figs. 24 and 25), it is possible to plot the data for the two orbits. The shaded areas are shown in detail in Figs. 26 and 27 for the 40 and 90 degrees yaw manoeuvres respectively. In both plots, there are the densities predicted with the DTM-2013 atmospheric model, SPARTA and panel methods. The solid lines characterize the densities estimated within the manoeuvre, whereas the dashed lines represent the values estimated outside the manoeuvres. For both the 40 and 90 degree attitude changes, it is possible to appreciate lower differences between the SPARTA densities. This is visible when the satellite changes to a perpendicular orientation with respect to the flow. Fig. 27, shows high agreement between

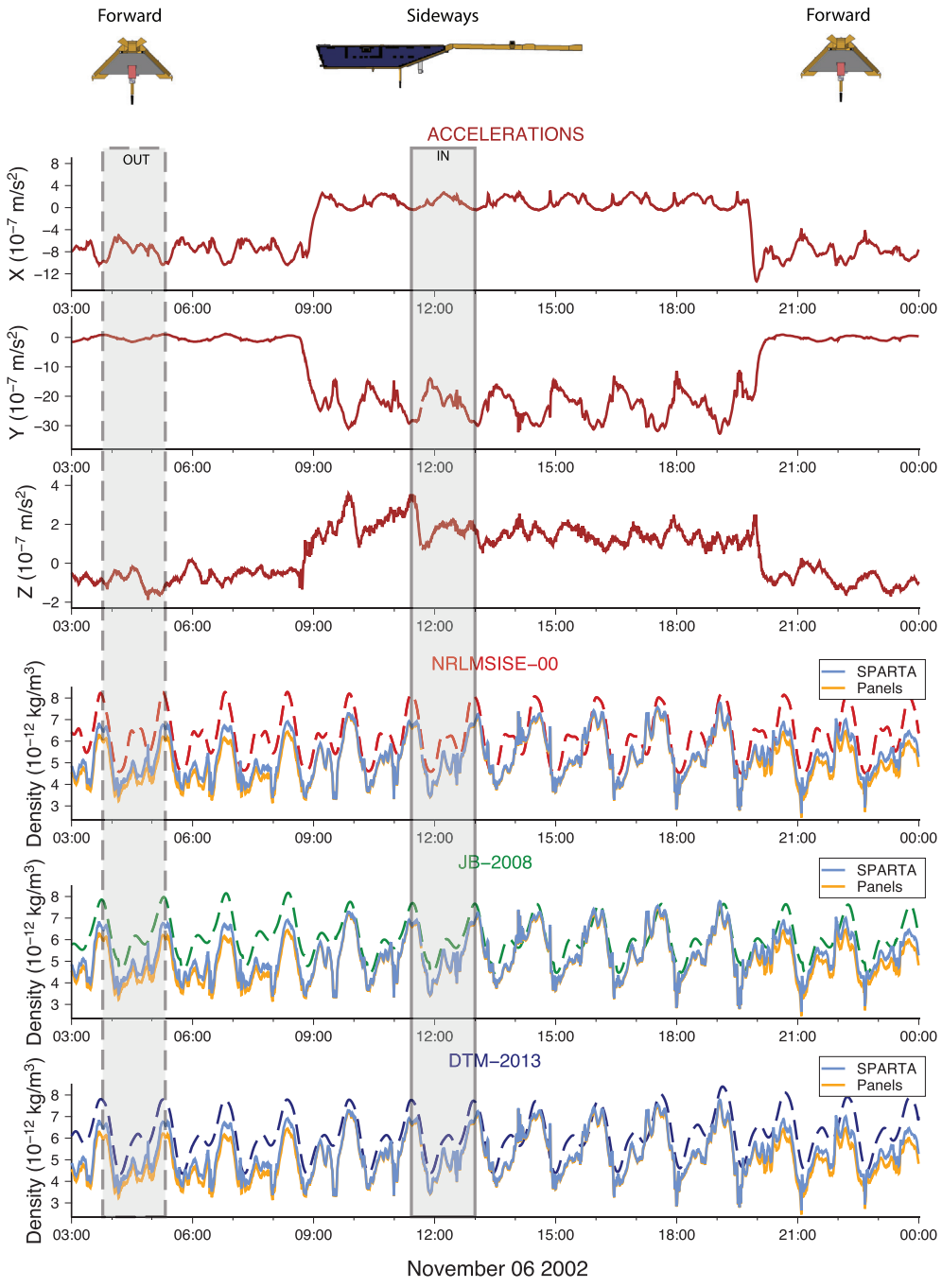

Fig. 28. CHAMP densities for panel method and SPARTA during 90 deg yaw manoeuvre on 2002-11-06. Comparison with three atmospheric models: NRLMSISE-00, JB-2008 and DTM-2013.

SPARTA densities and a very large discrepancy for the panel method, which reaches up to 40% of difference.

These findings are also confirmed for CHAMP. For this satellite, a 90 degree yaw manoeuvre has been selected. This sideways-flying attitude period occurred on 6th November 2002, between approximately 9:00 and 20:00 UTC, and it has already been investigated in Doornbos (2011). Similar to Swarm, Fig. 28 shows the accelerations and estimated densities for this manoeuvre. The solar activity was high and the data provided quite different densities also between short time windows. The results turn out to contain higher frequency information with respect to Swarm. This is mostly related to the smoothed GPS-derived accelerations used for Swarm. However, also in this case, a more stable trend for SPARTA densities is achieved within a few orbits. The panel method continues to have large discrepancies. This is highlighted by Fig. 29 which shows the densities as a function of the argument of

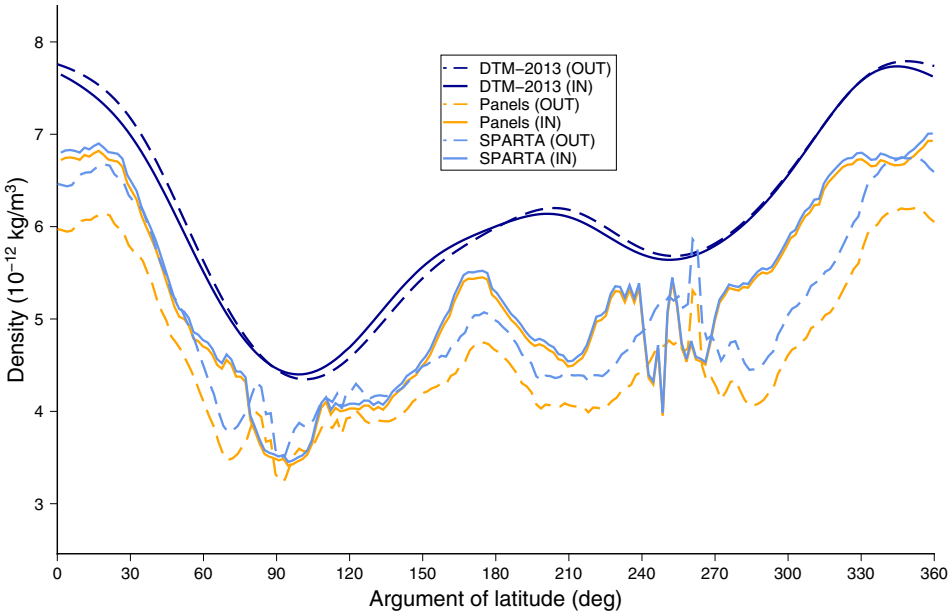

Fig. 29. CHAMP densities for panel method and SPARTA during 90 deg yaw manoeuvre on 2002-11-06. Comparison with DTM-2013. The line types correspond to the data equally marked in Fig. 28 for outside (dashed) and inside (solid) the analysed attitude manoeuvre.

latitude, which is the angle between the ascending node and the satellite along the orbit. For low arguments of latitude, there is a very similar trend between SPARTA densities. However, there is a relevant difference between solid and dashed lines for the panel approach. Discrepancies tend to increase for both methods after the second equator transit, but they get smaller again towards the end of the orbit. Larger differences are reached after crossing the descending equator position and in particular at the south pole. This is explained by the high variability of the thermosphere, especially for high solar activities for regions with complex atmospheric dynamics.

6. Conclusions and recommendations

This paper presents new thermospheric density estimations using accelerometer and GPS derived accelerations. High fidelity geometries have been designed using technical drawings and pre-launch photographs in order to raise as much as possible the accuracy level. Physics-based drag coefficients have been obtained as the outcome of a preliminary processing. Further processing of aerodynamic data sets has been applied in order to retrieve improved densities. A general improvement can be found comparing the average mean ratios between panels and SPARTA models with the atmospheric models. The reliability of the new model has been additionally verified with the manoeuvre analyses. This study shows an improvement in the consistency of densities through changes of attitude. New densities turned out to be higher than the panel method results. Indeed, differences of +11% for CHAMP, +5% for GRACE, +9% for GOCE and +32% for Swarm have been detected in this study. The improvement with respect to previous geometry modelling is especially relevant for Swarm and, in general, for satellites with complex shape. For GRACE, the achieved improvements resulted to be lower in magnitude, because of the simpler outer surfaces, which are easier to model also with the panel method approach. The weight of atmospheric models on the final results highlight different behaviours. Further research based on overlap analyses performed between different missions in the same time window will provide additional benefits. Together with a high fidelity gas-surface interactions model, densities and wind will be also improved. Based on the presented results, further research can now investigate and provide tools for gas-surface interactions models optimization and atmospheric models tuning. Different accommodation coefficients and GSI modellings based on the presented model will provide more consistent thermospheric density data sets, improved atmospheric models and accurate predictions of satellite drag.

Acknowledgements

This work was supported by the Netherlands Organisation for Scientific Research (NWO) project number ALW-GO/14-35. The authors would like to thank Steve Plimpton and Michael Gallis from SANDIA Laboratories for their support on SPARTA DSMC simulator. An additional acknowledgement goes to the European Space Agency for supporting the production of Swarm density products.

Appendix A. Comparison between SPARTA and technical drawing geometries

See Figs. A.1–A.6.

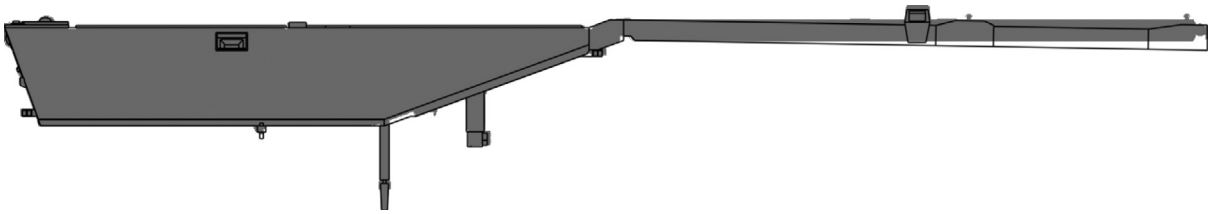

Fig. A.1. Comparison between technical drawing (shaded area) and SPARTA geometry model (black lines) for CHAMP. Inclination of boom has been modified from technical drawings by 1 deg (Luehr, 2000). Side view.

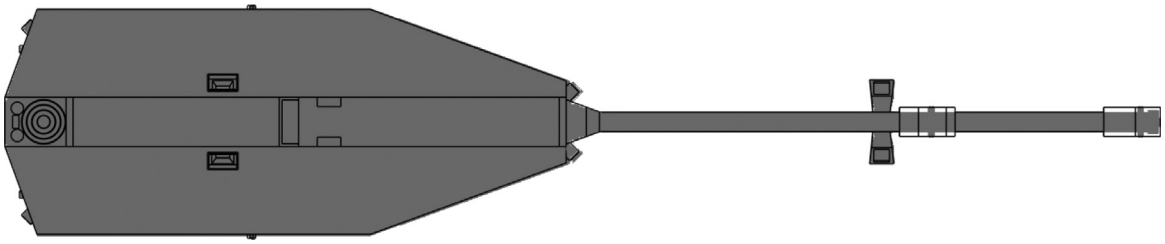

Fig. A.2. Comparison between technical drawing (shaded area) and SPARTA geometry model (black lines) for CHAMP. Larger SPARTA geometry areas are modelled to take into account covering materials, which are not included in the technical drawings. Top view.

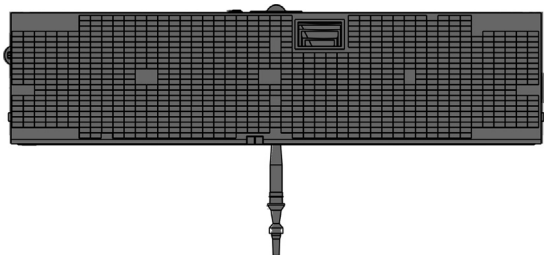

Fig. A.3. Comparison between technical drawing (shaded area) and SPARTA geometry model (black lines) for GRACE. Side view.

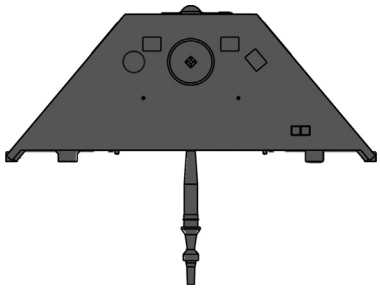

Fig. A.4. Comparison between technical drawing (shaded area) and SPARTA geometry model (black lines) for GRACE. Front view.

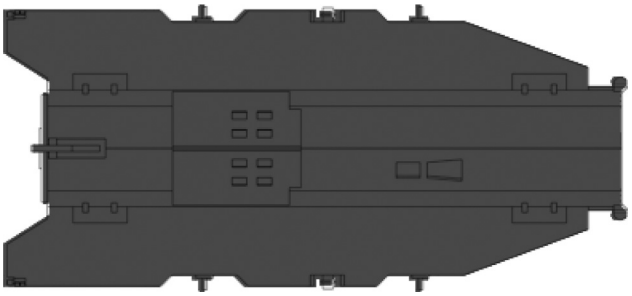

Fig. A.6. Comparison between technical drawing (shaded area) and SPARTA geometry model (black lines) for GOCE.

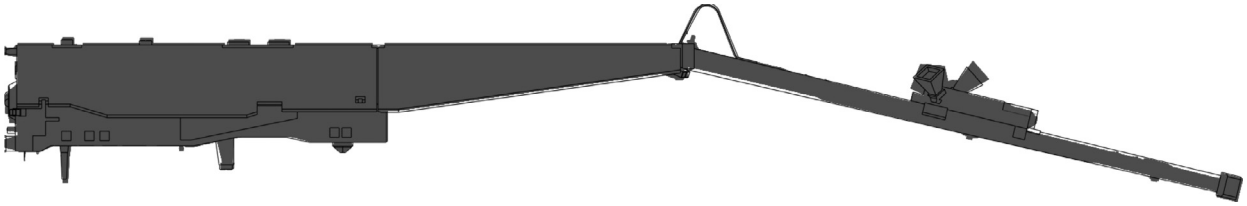

Fig. A.5. Comparison between technical drawing (shaded area) and SPARTA geometry model (black lines) for Swarm.

References

Astafyeva, E., Zakharenkova, I., Huba, J.D., Doornbos, E., van den IJssel, J., 2017. Global ionospheric and thermospheric effects of the June 2015 geomagnetic disturbances: multi-instrumental observations and modeling. J. Geophys. Res.: Space Phys. https://doi.org/10.1002/2017JA024174.

Bettadpur, S., 2007. Gravity Recovery and Climate Experiment Product Specification Document (Rev 4.5 – February 20, 2007). Tech. Rep. GRACE 327-720/CSR-GR-03-02. Center for Space Research, The University of Texas at Austin.

Bettadpur, S.V., 2012. GRACE Product Specification Document. Tech. Rep. GRACE 327-720 (CSR-GR-03-02). Center for Space Research, The University of Texas at Austin.

Bird, G.A., 1994. Molecular Gas Dynamics and the Direct Simulation of Gas Flows, vol. 42. ISBN: 9780198561958.

Bowman, B.R., Tobiska, K.W., Marcos, F.A., Huang, C.Y., Lin, C., Burke, W.F., 2008. A new empirical thermospheric density model JB-2008 using new solar and geomagnetic indices. In: AIAA/AAS Astrodynamics Specialist Conference and Exhibit 18–21 August 2008, Honolulu, Hawaii. No. AIAA 2008-6438.

Bruinsma, S., 2015. The DTM-2013 thermosphere model. J. Space Weather Space Clim. 5, A1. https://doi.org/10.1051/swsc/2015001.

Bruinsma, S., Biancale, R., 2003. Total densities derived from accelerometer data. J. Spacecraft Rockets 40, 230–236. https://doi.org/10.2514/2.3937.

Bruinsma, S., Tamagnan, D., Biancale, R., 2004. Atmospheric densities derived from CHAMP/STAR accelerometer observations. Planet. Space Sci. 52, 297–312. https://doi.org/10.1016/j.pss.2003.11.004.

Cometto, F., 2007. GOCE models data bank document (DCG No.: EN-18 April 30, 2007), GO-TN-AI-0081. Tech. rep., Alcatel Alenia Space.

Davis, D., 1960. Monte carlo calculation of molecular flow rates through a cylindrical elbow and pipes of other shapes. Appl. Phys. 30, 69–76, cited By 2.

Doornbos, E., 2011. Thermospheric Density and Wind Determination From Satellite Dynamics (Ph.D. thesis). Delft University of Technology. ISBN: 978-90-9026051-8.

Doornbos, E., Foerster, M., Fritsche, B., van Helleputte, T., van den IJssel, J., Koppenwallner, G., Luehr, H., Rees, D., Visser, P., 2009. Air density models derived from multi-satellite drag observations - final report. Tech. Rep. ESTEC contract 21022/07/NL/HE, DEOS/TU Delft scientific report 01/2009.

Doornbos, E., van den IJssel, J., Iorfida, E., 2017. GPS-derived density data for the Swarm satellites during the declining phase of the solar cycle. In: Fourth Swarm Science Meeting and Geodetic Missions Workshop, 20–24 March 2017, Banff, Canada. <http://old.esaconferencebureau.com/docs/default-source/17c04-docs/e-doornbos.pdf>.

Doornbos, E., van den IJssel, J., Luehr, H., Foerster, M., Koppenwallner, G., Bruinsma, S., Sutton, E., Forbes, J.M., Marcos, F., Perosanz, F., 2010. Neutral density and crosswind determination from arbitrarily oriented multiaxis accelerometers on satellites. J. Spacecraft Rockets 47, 580–589. https://doi.org/10.2514/1.48114.

Drob, D.P., Emmert, J.T., Crowley, G., Picone, J.M., Shepherd, G.G., Skinner, W., Hays, P., Niciejewski, R.J., Larsen, M., She, C.Y., Meriwether, J.W., Hernandez, G., Jarvis, M.J., Sipler, D.P., Tepley, C. A., O'Brien, M.S., Bowman, J.R., Wu, Q., Murayama, Y., Kawamura, S., Reid, I.M., Vincent, R.A., 2008. An empirical model of the Earth's horizontal wind fields: HWM07. J. Geophys. Res.: Space Phy. https://doi.org/10.1029/2008JA013668.

Drob, D.P., Emmert, J.T., Meriwether, J.W., Makela, J.J., Doornbos, E., Conde, M., Hernandez, G., Noto, J., Zawdie, K.A., McDonald, S.E., Huba, J.D., Klenzing, J.H., 2015. An update to the Horizontal Wind Model (HWM): the quiet time thermosphere. Earth Space Sci. https://doi.org/10.1002/2014EA000089.

Emmert, J.T., 2009. A long-term data set of globally averaged thermospheric total mass density. J. Geophys. Res.: Space Phys. 114 (6). https://doi.org/10.1029/2009JA014102.

Flury, J., Bettadpur, S., Tapley, B.D., 2008. Precise accelerometry onboard the GRACE gravity field satellite mission. Adv. Space Res. 42 (8), 1414–1423. https://doi.org/10.1016/j.asr.2008.05.004.

Gallis, M.A., Torczynski, J.R., Plimpton, S.J., Rader, D.J., Koehler, T., 2014. Direct simulation Monte Carlo: the quest for speed. In: AIP Conference Proceedings, vol. 1628, pp. 27–36. https://doi.org/10.1063/1.4902571.

Hammond, R., 2006. Satellite External Layout – DT0217691. Tech. rep., ASTRIUM.

Hess, C., 2001. GR00-000000A00A Grace S/C Flight Configuration. Tech. rep., Astrium GmbH.

Koppenwallner, G., 2009. Energy accommodation coefficient and momentum transfer modeling. Tech. Rep. HTG-TN-08-11, HTG, Katlenburg Lindau.

Luehr, H., 2000. Personal Communication on CH-IT-DID-0001. Tech. rep., Daimler-Chrysler Aerospace.

Luehr, H., 2002. CHAMP reference systems, transformations and standards. Tech. Rep. CH-GFZ-RS-002.

Mehta, P.M., McLaughlin, C.A., Sutton, E.K., 2013. Drag coefficient modeling for grace using direct simulation monte carlo. Adv. Space Res. 52 (12), 2035–2051. https://doi.org/10.1016/j.asr.2013.08.033.

Mehta, P.M., Walker, A.C., Sutton, E.K., Godinez, H.C., 2017. New density estimates derived using accelerometers on board the CHAMP and GRACE satellites. Space Weather 15 (4), 558–576. https://doi.org/10.1002/2016SW001562.

Moe, K., Moe, M.M., Rice, C.J., 2004. Simultaneous analysis of multi-instrument satellite measurements of atmospheric density. J. Spacecraft Rockets 41 (5), 849–853.

Pardini, C., Anselmo, L., Moe, K., Moe, M.M., 2010. Drag and energy accommodation coefficients during sunspot maximum. Adv. Space Res. 45 (5), 638–650. https://doi.org/10.1016/j.asr.2009.08.034.

Picone, J.M., Emmert, J.T., Lean, J.L., 2005. Thermospheric densities derived from spacecraft orbits: accurate processing of two-line element sets. J. Geophys. Res.: Space Phys. 110 (A3). https://doi.org/10.1029/2004JA010585.

Picone, J.M., Hedin, A.E., Drob, D.P., Aikin, A.C., 2001. NRLMSISE–00 empirical model of the atmosphere: statistical comparisons and scientific issues. J. Geophys. Res.: Space Phys. 107 (A12). https://doi.org/10.1029/2002JA009430, URL SIA 15–1–SIA 15–16 <https://agupubs.onlinelibrary.wiley.com/doi/pdf/10.1029/2002JA009430> .

Pilinski, M.D., 2011. Dynamic Gas-Surface Interaction Modeling for Satellite Aerodynamic Computations (Ph.D. thesis). University of Colorado at Boulder.

Pilinski, M.D., Argrow, B.M., Palo, S.E., 2013. Semiempirical model for satellite energy-accommodation coefficients. J. Spacecraft Rockets 47 (6), 951–956. https://doi.org/10.2514/1.49330.

Pilinski, M.D., Bowman, B.A., Palo, S.E., Forbes, J.M., Davis, B.L., Moore, R.G., Koehler, C., Sanders, B., 2016. Comparative analysis of satellite aerodynamics and its application to space-object identification. J. Spacecraft Rockets 53 (5), 1–11. https://doi.org/10.2514/1.A33482.

Schulz, H., 1999. CH-00-20/00.00 LAUNCH CONFIGURATION. Tech. rep., Daimler-Chrysler Aerospace.

Sentman, L., 1961a. Comparison of the exact and approximate methods for predicting free molecule aerodynamic coefficients. ARS J. 1, 1576–1579.

Sentman, L., 1961b. Free molecule flow theory and its application to the determination of aerodynamic forces. Tech. Rep. TR LMSC-448514. Lockheed Missile and Space Co., Sunnyvale, CA.

Severino, 2004a. G.O.C.E. Reference Axis. Tech. rep., Alenia Spazio S.p. A. Stabilimento di Torino.

Severino, 2004b. GOCE/Launcher Mechanical I/F. Tech. rep., Alenia Spazio S.p.A. Stabilimento di Torino.

Siemes, C., 2018. Swarm satellite thermo-optical properties and external geometry, ESA-EOPG-MOM-MO-15. Tech. rep., ESA. <https://earth.esa.int/documents/10174/2563139/Swarm_thermo-optical_properties_and_external_geometry.pdf>.

Siemes, C., de Teixeira da Encarnação, J., Doornbos, E., van den IJssel, J., Kraus, J., Pereštý, R., Grunwaldt, L., Apelbaum, G., Flury, J., Holmdahl Olsen, P.E., 2016. Swarm accelerometer data processing from raw accelerations to thermospheric neutral densities. Earth Planets Space 68 (1), 92. https://doi.org/10.1186/s40623-016-0474-5.

Sutton, E.K., 2008. Effects of Solar Disturbances on the Thermosphere Densities and Winds from CHAMP and GRACE Satellite Accelerometer Data (Ph.D. thesis). University of Colorado at Boulder.

Sutton, E.K., 2009. Normalized force coefficients for satellites with elongated shapes. J. Spacecraft Rockets 46 (1), 112–116. https://doi.org/10.2514/1.40940.

Van den IJssel, J., 2014. GPS-based Precise Orbit Determination and Accelerometer for Low Flying Satellites (Ph.D. thesis). Delft University of Technology.

Walker, A., Mehta, P.M., Koller, J., 2014. Drag coefficient model using the cercignani–lampis–lord gas–surface interaction model. J. Spacecraft Rockets 51 (5), 1544–1563. https://doi.org/10.2514/1.A32677.

Weimer, D.R., Sutton, E.K., Mlynczak, M.G., Hunt, L.A., 2016. Intercalibration of neutral density measurements for mapping the thermosphere. J. Geophys. Res.: Space Phys. 121 (6), 5975–5990. https://doi.org/10.1002/2016JA022691.

Wermuth, M., Montenbruck, O., van Helleputte, T., 2010. GPS high precision orbit determination software tools (GHOST);. In: 4th International Conference on Astrodynamics Tools and Techniques.